Isotropic Planar Layered Media

Mazin Mustafa

February 14, 2022

1 Introduction

In this document, we discuss the problem of planar layered structures consisting of isotropic media stratified against the z-axis as shown in Figure 1. We assume $N > 0$ layers defined with finite thicknesses numbered $1, \ldots, N$ ascending from top to bottom. Each layer $n \in [1, N]$ occupies the space $z_n \leq z \leq z_{n-1}$, hence the thickness is $d_n = z_{n-1} - z_n$. Note that each layer extends to infinity in the transverse x-y plane. The top layer $n = 1$ ends at z_0, while the bottom layer $n = N$ ends at z_N. This choice allows us to set numerical boundaries when computing the fields. One should note that this choice still allows us to define semi-infinite layers at $n = 1$ and $n = N$ by setting the appropriate boundaries values at z_0 and z_N, respectively. Moreover, each layer n is filled with isotropic medium specified by electric and magnetic constants ϵ_n and μ_n, respectively. In general, the media parameters take the form $\mu = \mu' - j\mu''$ and $\epsilon = \epsilon' - j\epsilon''$ without restrictions. In addition to this, we will allow homogeneous resistive sheets to be placed at the interfaces between layers. These resistive (conductive) sheets are modeled using the isotropic surface conductivities σ_n^s. Note that we don't allow σ_0^s nor σ_N^s since both these positions are reserved for numerical boundaries.

The EM problems to be solved here includes electric and magnetic current distributions, $\boldsymbol{J}$ and $\boldsymbol{M}$, to be placed inside the structure. We will only treat time-harmonic fields and assume the time dependency $e^{j\omega t}$. Thus, the rotation Maxwell's postulates are:

$$\begin{aligned} -\nabla \times \boldsymbol{E} &= j\omega\mu_0\mu\boldsymbol{H} + \boldsymbol{M} \\ \nabla \times \boldsymbol{H} &= j\omega\epsilon_0\epsilon\boldsymbol{E} + \boldsymbol{J} \end{aligned} \tag{1}$$

The transverse fields continuity boundary condition between two contiguous layers n and $n + 1$ are:

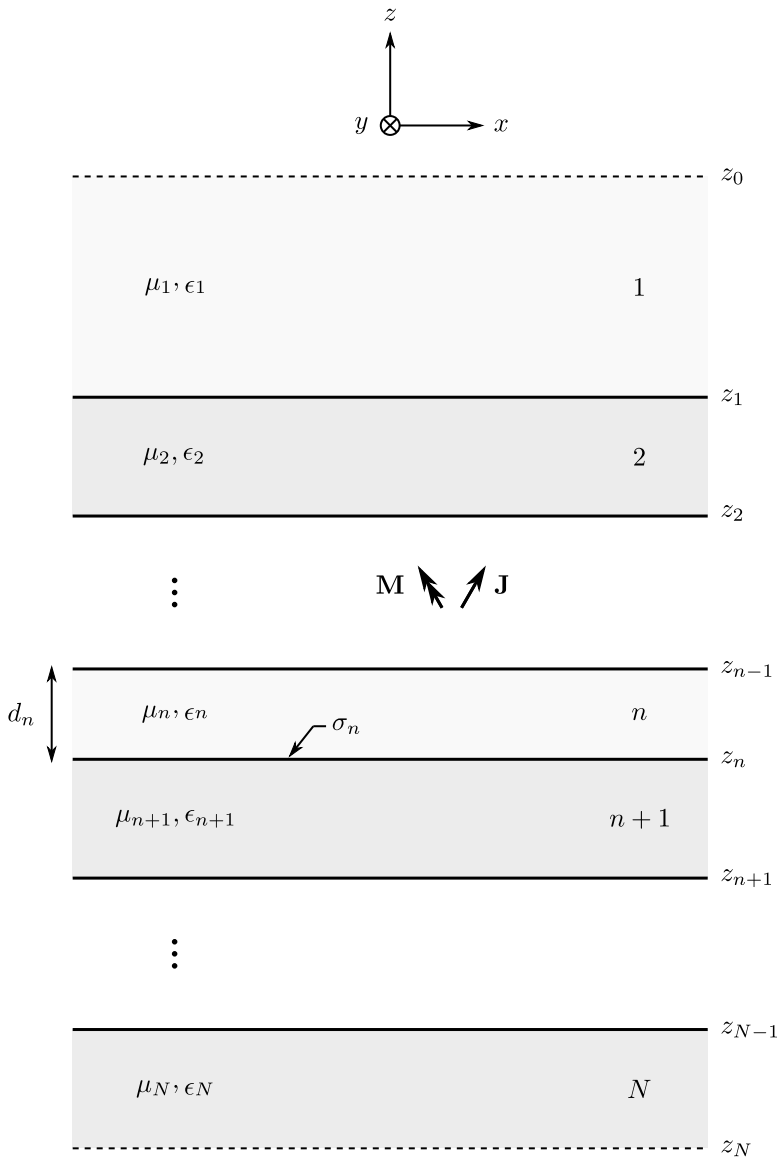

Figure 1: The configuration of planar layered media problem excited by point sources.

$$\begin{aligned}\hat{\boldsymbol{z}} \times \big[\boldsymbol{E}_n(z_n) - \boldsymbol{E}_{n+1}(z_n)\big] &= 0 \\ \hat{\boldsymbol{z}} \times \big[\boldsymbol{H}_n(z_n) - \boldsymbol{H}_{n+1}(z_n)\big] &= \sigma_n^s \boldsymbol{E}_n(z_n)\end{aligned} \tag{2}$$

Note that the normal fields jump boundary condition are automatically satisfied once the continuity is satisfied.

1.1 Problem Formulation

In this section, we will derive the differential equations to represent our problem using the elegant transmission line (TL) solution. For simplicity, we will drop the layer number notation temporarily and consider $\mu(z)$ and $\epsilon(z)$. Later, we will describe each layer's solution explicitly using the TL. We will start from the Maxwell's postulates, we decompose the expressions into transverse and longitudinal parts:

$$\begin{aligned}\nabla_t E_z - \partial_z \boldsymbol{E}_t &= j\omega\mu_0\mu(\boldsymbol{H}_t \times \hat{\boldsymbol{z}}) + \boldsymbol{M}_t \times \hat{\boldsymbol{z}} \\ \nabla_t H_z - \partial_z \boldsymbol{H}_t &= j\omega\epsilon_0\epsilon(\hat{\boldsymbol{z}} \times \boldsymbol{E}_t) + \hat{\boldsymbol{z}} \times \boldsymbol{J}_t\end{aligned} \tag{3}$$

$$\begin{aligned}j\omega\epsilon_0\epsilon E_z &= \hat{\boldsymbol{z}} \cdot \nabla_t \times \boldsymbol{H}_t - J_z \\ -j\omega\mu_0\mu H_z &= \hat{\boldsymbol{z}} \cdot \nabla_t \times \boldsymbol{E}_t + M_z\end{aligned} \tag{4}$$

The subscript t notation stands for the transverse fields components where $\nabla = \nabla_t + \partial_z \hat{\boldsymbol{z}}$. Since there is no variation on the transverse direction, we can apply the following 2D Fourier transform:

$$\begin{aligned}\tilde{f}(\boldsymbol{k}_\rho) &= \int_{-\infty}^{\infty}\int_{-\infty}^{\infty} f(\boldsymbol{\rho}) e^{j\boldsymbol{k}_\rho \cdot \boldsymbol{\rho}} d\boldsymbol{\rho} \\ f(\boldsymbol{\rho}) &= \frac{1}{(2\pi)^2}\int_{-\infty}^{\infty}\int_{-\infty}^{\infty} \tilde{f}(\boldsymbol{k}_\rho) e^{-j\boldsymbol{k}_\rho \cdot \boldsymbol{\rho}} d\boldsymbol{k}_\rho\end{aligned} \tag{5}$$

In the spectral domain $\boldsymbol{k}_\rho = k_\rho[\cos(\xi)\hat{\boldsymbol{x}} + \sin(\xi)\hat{\boldsymbol{y}}]$ as shown in Figure 2, and this results in $\nabla_t \longrightarrow -j\boldsymbol{k}_\rho$. We will also omit the $\boldsymbol{k}_\rho$ dependency in the fields expressions. After applying the Fourier transform and combining the results we obtain:

$$\begin{aligned}\partial_z \tilde{\boldsymbol{E}}_t &= \frac{1}{j\omega\epsilon_0\epsilon}[k^2 \underline{\boldsymbol{I}}_t - \boldsymbol{k}_\rho \boldsymbol{k}_\rho] \cdot (\tilde{\boldsymbol{H}}_t \times \hat{\boldsymbol{z}}) + \frac{\boldsymbol{k}_\rho}{\omega\epsilon_0\epsilon}\tilde{J}_z - \tilde{\boldsymbol{M}}_t \times \hat{\boldsymbol{z}} \\ \partial_z \tilde{\boldsymbol{H}}_t &= \frac{1}{j\omega\mu_0\mu}[k^2 \underline{\boldsymbol{I}}_t - \boldsymbol{k}_\rho \boldsymbol{k}_\rho] \cdot (\hat{\boldsymbol{z}} \times \tilde{\boldsymbol{E}}_t) + \frac{\boldsymbol{k}_\rho}{\omega\mu_0\mu}\tilde{M}_z + \tilde{\boldsymbol{J}}_t \times \hat{\boldsymbol{z}}\end{aligned} \tag{6}$$

The wavenumber $k = k_0\sqrt{\mu\epsilon}$ and $k_0 = \omega/c_0 = 2\pi/\lambda_0$. The speed of light in free-space is $c_0 = 1/\sqrt{\mu_0\epsilon_0}$ and the wavelength is λ_0. Also, $\underline{\boldsymbol{I}}_t$ is the transverse unit dyadic. We also assume the wavevector $\boldsymbol{k} = \boldsymbol{k}_\rho + k_z\hat{\boldsymbol{z}}$. In the spectral domain, we can use the definition of $\boldsymbol{k}_\rho$ as shown in Figure 2 in order to decompose the fields components as follows:

$$\begin{aligned} \tilde{\boldsymbol{E}}_t &= V^e\hat{\boldsymbol{u}} + V^h\hat{\boldsymbol{v}} \\ \tilde{\boldsymbol{H}}_t &= I^e\hat{\boldsymbol{v}} - I^h\hat{\boldsymbol{u}} \end{aligned} \tag{7}$$

$$\begin{aligned} \hat{\boldsymbol{z}} \times \tilde{\boldsymbol{E}}_t &= V^e\hat{\boldsymbol{v}} - V^h\hat{\boldsymbol{u}} \\ \tilde{\boldsymbol{H}}_t \times \hat{\boldsymbol{z}} &= I^e\hat{\boldsymbol{u}} + I^h\hat{\boldsymbol{v}} \end{aligned} \tag{8}$$

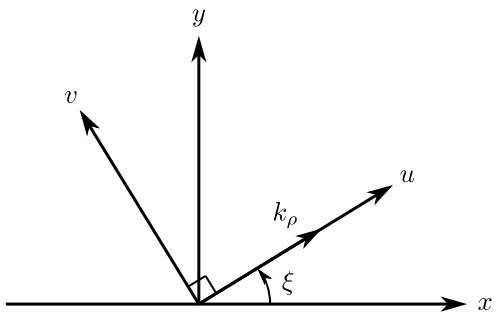

Figure 2: Spectral domain orthonormal set of vectors $(\hat{\boldsymbol{u}}, \hat{\boldsymbol{v}}, \hat{\boldsymbol{z}})$. The transverse wavevector is defined as $\boldsymbol{k}_\rho = k_\rho\hat{\boldsymbol{u}}$.

This choice ensures the decomposition of fields into e and h modes according to the transverse wavevector $\boldsymbol{k}_\rho$ which follows the physical meanings of these modes. Substituting the previous definitions into (6), we obtain the systems:

$$\begin{aligned} \partial_z V^\alpha &= -jk_z Z^\alpha I^\alpha + v^\alpha \\ \partial_z I^\alpha &= -jk_z Y^\alpha V^\alpha + i^\alpha \end{aligned} \tag{9}$$

The notation α is applicable for both modes e and h. In the above, we defined $k_z = \sqrt{k^2 - k_\rho^2}$, and the impedances $Z^e = k_z/\omega\epsilon_0\epsilon$ and $Z^h = \omega\mu_0\mu/k_z$. Also, $Z^\alpha = 1/Y^\alpha$ and $Z^eZ^h = \eta^2$, where the intrinsic impedance $\eta = \eta_0\sqrt{\mu/\epsilon}$ and the free-space $\eta_0 = \sqrt{\mu_0/\epsilon_0}$. The sources in (9) are given as follows:

$$\begin{aligned} v^e &= \frac{k_\rho}{\omega\epsilon_0\epsilon}\tilde{J}_z - \tilde{M}_v \quad , \quad v^h = \tilde{M}_u \\ i^h &= -\frac{k_\rho}{\omega\mu_0\mu}\tilde{M}_z - \tilde{J}_v \quad , \quad i^e = -\tilde{J}_u \end{aligned} \tag{10}$$

The system of equations in (9) represents TLs excited by series voltage sources v and shunt current sources i. This problem can be treated efficiently using Transmission Line Green Functions (TLGFs). Hence, we solve the systems for point sources $\delta(z-z')$ as follows:

$$\begin{aligned} \partial_z V_v^\alpha &= -jk_z Z I_v^\alpha + \delta(z-z') \\ \partial_z I_v^\alpha &= -jk_z Y V_v^\alpha \end{aligned} \tag{11}$$

$$\begin{aligned} \partial_z V_i^\alpha &= -jk_z Z I_i^\alpha \\ \partial_z I_i^\alpha &= -jk_z Y V_i^\alpha + \delta(z-z') \end{aligned} \tag{12}$$

The subscripts v and i correspond to the source type. A TL analogy of this problem is illustrated in Figure 3. In our solution, we will always assume the excitation to be located at z' inside layer $m \in [1, N]$.

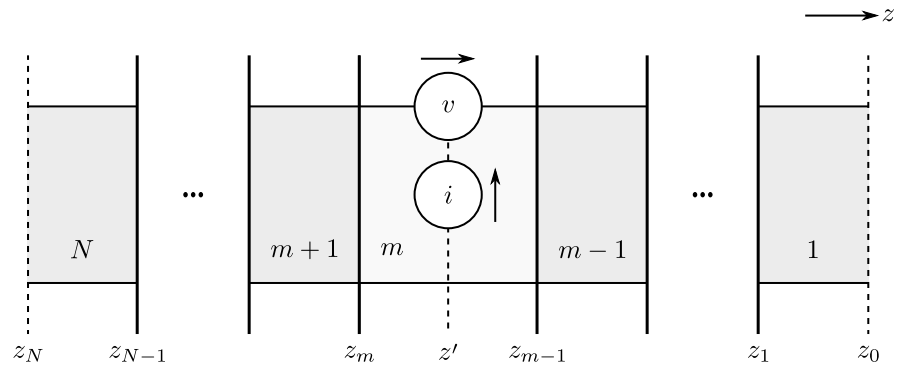

Figure 3: Transmission line representation of the systems in (9) applicable for both e and h modes.

The voltages $V_s^\alpha(z|z')$ and currents $I_s^\alpha(z|z')$ are the TLGFs, where the source type s is either v or i. Utilizing the superposition, we may convolve the sources definitions from (10) with the TLGFs along z' and obtain:

$$\begin{aligned} V^\alpha(z) &= \langle V_v^\alpha(z|z'), v^\alpha(z')\rangle + \langle V_i^\alpha(z|z'), i^\alpha(z')\rangle \\ I^\alpha(z) &= \langle I_v^\alpha(z|z'), v^\alpha(z')\rangle + \langle I_i^\alpha(z|z'), i^\alpha(z')\rangle \end{aligned} \tag{13}$$

Thus, the total spectral fields can be evaluated as:

$$\begin{aligned}\tilde{\boldsymbol{E}} &= V^e\hat{\boldsymbol{u}} + V^h\hat{\boldsymbol{v}} - \frac{1}{j\omega\epsilon_0\epsilon}\Big(jk_\rho I^e + \tilde{J}_z\Big)\hat{\boldsymbol{z}} \\ \tilde{\boldsymbol{H}} &= -I^h\hat{\boldsymbol{u}} + I^e\hat{\boldsymbol{v}} + \frac{1}{j\omega\mu_0\mu}\Big(jk_\rho V^h - \tilde{M}_z\Big)\hat{\boldsymbol{z}}\end{aligned} \tag{14}$$

Assuming that the TLGFs were found, we can express the TL quantities as follows:

$$\begin{aligned}V^e &= -\langle V_i^e, \tilde{J}_u\rangle - \langle V_v^e, \tilde{M}_v\rangle + \langle V_v^e\frac{k_\rho}{\omega\epsilon_0\epsilon}, \tilde{J}_z\rangle \\ I^e &= -\langle I_i^e, \tilde{J}_u\rangle - \langle I_v^e, \tilde{M}_v\rangle + \langle I_v^e\frac{k_\rho}{\omega\epsilon_0\epsilon}, \tilde{J}_z\rangle \\ V^h &= \langle V_v^h, \tilde{M}_u\rangle - \langle V_i^h, \tilde{J}_v\rangle - \langle V_i^h\frac{k_\rho}{\omega\mu_0\mu}, \tilde{M}_z\rangle \\ I^h &= \langle I_v^h, \tilde{M}_u\rangle - \langle I_i^h, \tilde{J}_v\rangle - \langle I_i^h\frac{k_\rho}{\omega\mu_0\mu}, \tilde{M}_z\rangle\end{aligned} \tag{15}$$

It is possible to write the spectral domain fields in compact form using Dyadic Green Functions (DGFs) as follows:

$$\begin{aligned}\tilde{\boldsymbol{E}} &= \langle\underline{\tilde{\boldsymbol{G}}}^{EJ}; \tilde{\boldsymbol{J}}\rangle + \langle\underline{\tilde{\boldsymbol{G}}}^{EM}; \tilde{\boldsymbol{M}}\rangle \\ \tilde{\boldsymbol{H}} &= \langle\underline{\tilde{\boldsymbol{G}}}^{HJ}; \tilde{\boldsymbol{J}}\rangle + \langle\underline{\tilde{\boldsymbol{G}}}^{HM}; \tilde{\boldsymbol{M}}\rangle\end{aligned} \tag{16}$$

Using(15) and (14), the spectral domain DGFs are:

$$\begin{aligned}\underline{\tilde{\boldsymbol{G}}}^{EJ} = &-V_i^e\hat{\boldsymbol{u}}\hat{\boldsymbol{u}} - V_i^h\hat{\boldsymbol{v}}\hat{\boldsymbol{v}} + \frac{k_\rho}{\omega\epsilon_0\epsilon}I_i^e\hat{\boldsymbol{z}}\hat{\boldsymbol{u}} + \frac{k_\rho}{\omega\epsilon_0\epsilon'}V_v^e\hat{\boldsymbol{u}}\hat{\boldsymbol{z}} \\ &- \frac{1}{j\omega\epsilon_0\epsilon'}\Big[\frac{jk_\rho^2}{\omega\epsilon_0\epsilon}I_v^e + \delta(z-z')\Big]\hat{\boldsymbol{z}}\hat{\boldsymbol{z}}\end{aligned} \tag{17}$$

$$\underline{\tilde{\boldsymbol{G}}}^{EM} = - V_v^e\hat{\boldsymbol{u}}\hat{\boldsymbol{v}} + V_v^h\hat{\boldsymbol{v}}\hat{\boldsymbol{u}} + \frac{k_\rho}{\omega\epsilon_0\epsilon}I_v^e\hat{\boldsymbol{z}}\hat{\boldsymbol{v}} - \frac{k_\rho}{\omega\mu_0\mu'}V_i^h\hat{\boldsymbol{v}}\hat{\boldsymbol{z}} \tag{18}$$

$$\underline{\tilde{\boldsymbol{G}}}^{HJ} = I_i^h\hat{\boldsymbol{u}}\hat{\boldsymbol{v}} - I_i^e\hat{\boldsymbol{v}}\hat{\boldsymbol{u}} - \frac{k_\rho}{\omega\mu_0\mu}V_i^h\hat{\boldsymbol{z}}\hat{\boldsymbol{v}} + \frac{k_\rho}{\omega\epsilon_0\epsilon'}I_v^e\hat{\boldsymbol{v}}\hat{\boldsymbol{z}} \tag{19}$$

$$\begin{aligned}\underline{\tilde{\boldsymbol{G}}}^{HM} = &-I_v^h \hat{\boldsymbol{u}}\hat{\boldsymbol{u}} - I_v^e \hat{\boldsymbol{v}}\hat{\boldsymbol{v}} + \frac{k_\rho}{\omega\mu_0\mu} V_v^h \hat{\boldsymbol{z}}\hat{\boldsymbol{u}} + \frac{k_\rho}{\omega\mu_0\mu'} I_i^h \hat{\boldsymbol{u}}\hat{\boldsymbol{z}} \\ &- \frac{1}{j\omega\mu_0\mu'}\Big[\frac{jk_\rho^2}{\omega\mu_0\mu} V_i^h + \delta(z-z')\Big]\hat{\boldsymbol{z}}\hat{\boldsymbol{z}}\end{aligned} \tag{20}$$

Where $\mu' = \mu(z')$ and $\epsilon' = \epsilon(z')$.

1.2 Spatial Dyadic Green Functions

In order to obtain the spatial domain fields, will consider evaluating the spectral domain DGFs inverse 2D Fourier transform. Here, we consider point sources located at $\boldsymbol{r'} = z'\hat{\boldsymbol{z}}$. This choice simplifies the derivation since the sources lie at $\rho = 0$. Nevertheless, we can shift the DGFs by $\boldsymbol{\rho'}$ to represent point sources at any location in the space. The inverse Fourier transform can be re-written as follows:

$$f(\boldsymbol{\rho}) = \mathcal{F}^{-1}\{\tilde{f}(\boldsymbol{k}_\rho)\} = \frac{1}{(2\pi)^2}\int_0^{2\pi}\int_0^{\infty} \tilde{f}(k_\rho,\xi) e^{-jk_\rho\rho\cos(\xi-\varphi)} k_\rho dk_\rho d\xi \tag{21}$$

It is possible to reduce the 2D integrals into Sommerfeld Integrals (SIs) as defined in (22) when $\tilde{f}(k_\rho,\xi) = \tilde{f}(k_\rho)$.

$$S_n\{\tilde{f}(k_\rho)\} = \frac{1}{2\pi}\int_0^{\infty} \tilde{f}(k_\rho) J_n(k_\rho\rho) k_\rho dk_\rho \tag{22}$$

This requires removing the ξ dependency from the expressions in (17)-(20). Thus, considering the following relation:

$$\frac{1}{2\pi}\int_{-\pi}^{\pi} e^{-jn\xi} e^{-jz\cos(\xi-\vartheta)} d\xi = (-j)^n J_n(z) e^{-jn\vartheta} \tag{23}$$

It is possible to re-write the following inverse Fourier transforms in terms of SIs as follows:

$$\begin{aligned}\mathcal{F}^{-1}\{\cos(\xi)\tilde{f}(k_\rho)\} &= -j\cos(\varphi) S_1\{\tilde{f}(k_\rho)\} \\ \mathcal{F}^{-1}\{\sin(\xi)\tilde{f}(k_\rho)\} &= -j\sin(\varphi) S_1\{\tilde{f}(k_\rho)\} \\ \mathcal{F}^{-1}\{\cos^2(\xi)\tilde{f}(k_\rho)\} &= \frac{1}{2}S_0\{\tilde{f}(k_\rho)\} - \frac{\cos(2\varphi)}{2} S_2\{\tilde{f}(k_\rho)\} \\ \mathcal{F}^{-1}\{\sin^2(\xi)\tilde{f}(k_\rho)\} &= \frac{1}{2}S_0\{\tilde{f}(k_\rho)\} + \frac{\cos(2\varphi)}{2} S_2\{\tilde{f}(k_\rho)\} \\ \mathcal{F}^{-1}\{\sin(\xi)\cos(\xi)\tilde{f}(k_\rho)\} &= \frac{\sin(2\varphi)}{2} S_2\{\tilde{f}(k_\rho)\}\end{aligned} \tag{24}$$

The ξ dependency comes from the spectral unit vectors $\hat{\boldsymbol{u}}$ and $\hat{\boldsymbol{v}}$:

$$\begin{aligned}\hat{\boldsymbol{u}} &= \cos(\xi)\hat{\boldsymbol{x}} + \sin(\xi)\hat{\boldsymbol{y}} \\ \hat{\boldsymbol{v}} &= -\sin(\xi)\hat{\boldsymbol{x}} + \cos(\xi)\hat{\boldsymbol{y}}\end{aligned} \tag{25}$$

Note that the above relations when applied to obtain the corresponding Cartesian coordinates dyadic components only result in $\cos(\xi)$, $\sin(\xi)$, $\cos^2(\xi)$, $\sin^2(\xi)$, and $\sin(\xi)\cos(\xi)$ coefficients. This makes the relations in (24) enough to handle all the DFGs components as listed below.

$$G_{xx}^{EJ}(\rho,\varphi,z|z') = -\frac{1}{2}S_0\{V_i^e + V_i^h\} + \frac{\cos(2\varphi)}{2}S_2\{V_i^e - V_i^h\} \tag{26}$$

$$G_{xy}^{EJ}(\rho,\varphi,z|z') = \frac{\sin(2\varphi)}{2}S_2\{V_i^e - V_i^h\} \tag{27}$$

$$G_{yx}^{EJ}(\rho,\varphi,z|z') = \frac{\sin(2\varphi)}{2}S_2\{V_i^e - V_i^h\} \tag{28}$$

$$G_{yy}^{EJ}(\rho,\varphi,z|z') = -\frac{1}{2}S_0\{V_i^e + V_i^h\} - \frac{\cos(2\varphi)}{2}S_2\{V_i^e - V_i^h\} \tag{29}$$

$$G_{xz}^{EJ}(\rho,\varphi,z|z') = \frac{\eta_0}{jk_0\epsilon'}\cos(\varphi)S_1\{k_\rho V_v^e\} \tag{30}$$

$$G_{yz}^{EJ}(\rho,\varphi,z|z') = \frac{\eta_0}{jk_0\epsilon'}\sin(\varphi)S_1\{k_\rho V_v^e\} \tag{31}$$

$$G_{zx}^{EJ}(\rho,\varphi,z|z') = \frac{\eta_0}{jk_0\epsilon}\cos(\varphi)S_1\{k_\rho I_i^e\} \tag{32}$$

$$G_{zy}^{EJ}(\rho,\varphi,z|z') = \frac{\eta_0}{jk_0\epsilon}\sin(\varphi)S_1\{k_\rho I_i^e\} \tag{33}$$

$$G_{zz}^{EJ}(\rho,\varphi,z|z') = -\frac{\eta_0^2}{k_0^2\epsilon\epsilon'}S_0\{k_\rho^2 I_v^e\} - \frac{\eta_0}{jk_0\epsilon}\delta(\rho)\delta(z-z') \tag{34}$$

$$G_{xx}^{HJ}(\rho,\varphi,z|z') = \frac{\sin(2\varphi)}{2}S_2\{I_i^h - I_i^e\} \tag{35}$$

$$G_{xy}^{HJ}(\rho,\varphi,z|z') = \frac{1}{2}S_0\{I_i^h + I_i^e\} - \frac{\cos(2\varphi)}{2}S_2\{I_i^h - I_i^e\} \tag{36}$$

$$G_{yx}^{HJ}(\rho,\varphi,z|z') = -\frac{1}{2}S_0\{I_i^h + I_i^e\} - \frac{\cos(2\varphi)}{2}S_2\{I_i^h - I_i^e\} \tag{37}$$

$$G_{yy}^{HJ}(\rho,\varphi,z|z') = -\frac{\sin(2\varphi)}{2}S_2\{I_i^h - I_i^e\} \tag{38}$$

$$G_{xz}^{HJ}(\rho,\varphi,z|z') = -\frac{\eta_0}{jk_0\epsilon'}\sin(\varphi)S_1\{k_\rho I_v^e\} \tag{39}$$

$$G_{yz}^{HJ}(\rho,\varphi,z|z') = \frac{\eta_0}{jk_0\epsilon'}\cos(\varphi)S_1\{k_\rho I_v^e\} \tag{40}$$

$$G_{zx}^{HJ}(\rho,\varphi,z|z') = \frac{1}{j\eta_0 k_0\mu}\sin(\varphi)S_1\{k_\rho V_i^h\} \tag{41}$$

$$G_{zy}^{HJ}(\rho,\varphi,z|z') = -\frac{1}{j\eta_0 k_0\mu}\cos(\varphi)S_1\{k_\rho V_i^h\} \tag{42}$$

$$G_{zz}^{HJ}(\rho,\varphi,z|z') = 0 \tag{43}$$

$$G_{xx}^{EM}(\rho,\varphi,z|z') = -\frac{\sin(2\varphi)}{2}S_2\{V_v^e - V_v^h\} \tag{44}$$

$$G_{xy}^{EM}(\rho,\varphi,z|z') = -\frac{1}{2}S_0\{V_v^e + V_v^h\} + \frac{\cos(2\varphi)}{2}S_2\{V_v^e - V_v^h\} \tag{45}$$

$$G_{yx}^{EM}(\rho,\varphi,z|z') = \frac{1}{2}S_0\{V_v^e + V_v^h\} + \frac{\cos(2\varphi)}{2}S_2\{V_v^e - V_v^h\} \tag{46}$$

$$G_{yy}^{EM}(\rho,\varphi,z|z') = \frac{\sin(2\varphi)}{2}S_2\{V_v^e - V_v^h\} \tag{47}$$

$$G_{xz}^{EM}(\rho,\varphi,z|z') = \frac{1}{j\eta_0 k_0\mu'}\sin(\varphi)S_1\{k_\rho V_i^h\} \tag{48}$$

$$G_{yz}^{EM}(\rho,\varphi,z|z') = -\frac{1}{j\eta_0 k_0\mu'}\cos(\varphi)S_1\{k_\rho V_i^h\} \tag{49}$$

$$G_{zx}^{EM}(\rho,\varphi,z|z') = \frac{j\eta_0}{k_0\epsilon}\sin(\varphi)S_1\{k_\rho I_v^e\} \tag{50}$$

$$G_{zy}^{EM}(\rho,\varphi,z|z') = -\frac{j\eta_0}{k_0\epsilon}\cos(\varphi)S_1\{k_\rho I_v^e\} \tag{51}$$

$$G_{zz}^{EM}(\rho,\varphi,z|z') = 0 \tag{52}$$

$$G_{xx}^{HM}(\rho,\varphi,z|z') = -\frac{1}{2}S_0\{I_v^h + I_v^e\} + \frac{\cos(2\varphi)}{2}S_2\{I_v^h - I_v^e\} \tag{53}$$

$$G_{xy}^{HM}(\rho,\varphi,z|z') = \frac{\sin(2\varphi)}{2}S_2\{I_v^h - I_v^e\} \tag{54}$$

$$G_{yx}^{HM}(\rho,\varphi,z|z') = \frac{\sin(2\varphi)}{2}S_2\{I_v^h - I_v^e\} \tag{55}$$

$$G_{yy}^{HM}(\rho,\varphi,z|z') = -\frac{1}{2}S_0\{I_v^h + I_v^e\} - \frac{\cos(2\varphi)}{2}S_2\{I_v^h - I_v^e\} \tag{56}$$

$$G_{xz}^{HM}(\rho,\varphi,z|z') = \frac{1}{j\eta_0 k_0\mu'}\cos(\varphi)S_1\{k_\rho I_i^h\} \tag{57}$$

$$G_{yz}^{HM}(\rho,\varphi,z|z') = \frac{1}{j\eta_0 k_0\mu'}\sin(\varphi)S_1\{k_\rho I_i^h\} \tag{58}$$

$$G_{zx}^{HM}(\rho,\varphi,z|z') = \frac{1}{j\eta_0 k_0\mu}\cos(\varphi)S_1\{k_\rho V_v^h\} \tag{59}$$

$$G_{zy}^{HM}(\rho,\varphi,z|z') = \frac{1}{j\eta_0 k_0\mu}\sin(\varphi)S_1\{k_\rho V_v^h\} \tag{60}$$

$$G_{zz}^{HM}(\rho,\varphi,z|z') = -\frac{1}{\eta_0^2 k_0^2\mu\mu'}S_0\{k_\rho^2 V_i^h\} - \frac{1}{j\eta_0 k_0\mu}\delta(\rho)\delta(z-z') \tag{61}$$

Where μ' and ϵ' are the media parameters at z'. For arbitrary location of sources, the following replacements can be applied:

$$\begin{aligned}\rho &\longrightarrow \varrho = \sqrt{(x-x')^2 + (y-y')^2} \\ \varphi &\longrightarrow \phi = \tan^{-1}\left[\frac{y-y'}{x-x'}\right]\end{aligned} \tag{62}$$

2 Transmission Line Solution

The TL solutions require solving the differential equations systems in (9). The solutions are subject to the boundary conditions in (2). In the spectral domain, we write these conditions as follows:

$$\begin{aligned} V^{\alpha}_{n+1}(z_n) - V^{\alpha}_{n}(z_n) &= 0 \\ I^{\alpha}_{n+1}(z_n) - I^{\alpha}_{n}(z_n) &= \sigma^{s}_{n} V^{\alpha}_{n}(z_n) \end{aligned} \tag{63}$$

$$\begin{aligned} V^{\alpha}_{n-1}(z_{n-1}) - V^{\alpha}_{n}(z_{n-1}) &= 0 \\ I^{\alpha}_{n-1}(z_{n-1}) - I^{\alpha}_{n}(z_{n-1}) &= -\sigma^{s}_{n-1} V^{\alpha}_{n}(z_{n-1}) \end{aligned} \tag{64}$$

The above boundaries can be applied between two contingent layers. The boundary conditions at z_0 and z_N will be used to represent the terminations choices. This is achieved by setting $\overrightarrow{\Gamma}_1$ and $\overleftarrow{\Gamma}_N$ to 0, -1, and 1 for semi-infinite, PEC, and PMC terminations, respectively. One can also specify an impedance termination, but this choice doesn't have any practical meaning as far we are concerned. For simplicity, the mode type α will be dropped since the same solution is applicable to both modes e and h. The TL consists of N sections corresponding to each layer in the configuration with the same longitudinal dimensions. An example of section n is illustrated in Figure 4 with reflection coefficients $\overleftarrow{\Gamma}_n$ and $\overrightarrow{\Gamma}_n$ definitions. The reflection coefficients $\overleftarrow{\Gamma}'$ and $\overrightarrow{\Gamma}'$ are defined from the reference point z'. The characteristic impedance of each section is Z_n and the propagation constant is k_{zn}. Moreover, we define the electrical length $\Theta_n = k_{zn} d_n$.

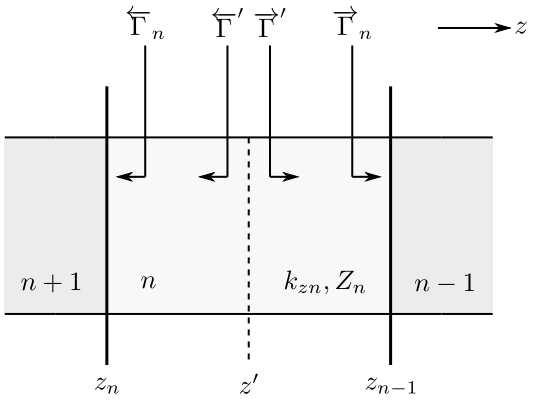

Figure 4: TL section n definition with source (reference) point z'.

In order to obtain the TLGFs, we either substitute $v = 1$ and $i = 0$ for (V_v, I_v), or $v = 0$ and $i = 1$ for (V_i, I_i). Here, z' is assumed to exist in

section $m \in [1, N]$ as discussed earlier but this doesn't prevent us from using the notation to describe various solutions. This choice allows two types of sections solutions, namely source-free ($n \neq m$) and source-excited ($n = m$) solutions. Also, the source-free solution by itself can be divided into two cases: down-looking ($n > m$) and up-looking ($n < m$) cases.

According to the problems in (11) and (12), it is possible to postulate the following solutions for any section n:

$$V_n(z) = \begin{cases} V_n^+(z) = V_n^+[e^{-jk_{zn}(z-z')} + \overrightarrow{\Gamma}' e^{+jk_{zn}(z-z')}] & , z > z' \\ V_n^-(z) = V_n^-[e^{+jk_{zn}(z-z')} + \overleftarrow{\Gamma}' e^{-jk_{zn}(z-z')}] & , z < z' \end{cases} \tag{65}$$

$$I_n(z) = \begin{cases} I_n^+(z) = +Y_n V_n^+[e^{-jk_{zn}(z-z')} - \overrightarrow{\Gamma}' e^{+jk_{zn}(z-z')}] & , z > z' \\ I_n^-(z) = -Y_n V_n^-[e^{+jk_{zn}(z-z')} - \overleftarrow{\Gamma}' e^{-jk_{zn}(z-z')}] & , z < z' \end{cases} \tag{66}$$

Later, we will utilize z' to describe the different solutions. Also, note the following relation between the reflections coefficients:

$$\begin{aligned} \overrightarrow{\Gamma}' &= \overrightarrow{\Gamma}_n e^{-j2k_{zn}(z_{n-1}-z')} \\ \overleftarrow{\Gamma}' &= \overleftarrow{\Gamma}_n e^{-j2k_{zn}(z'-z_n)} \end{aligned} \tag{67}$$

2.1 Source-Excited Solution ($n = m$)

In this type, the solutions in (65) and (66) can be used directly. The jump conditions at $z = z'$ are then enforced as in (68). Here, the physical location of the point source is z'.

$$\begin{aligned} V_n^+(z') - V_n^-(z') &= v \\ I_n^+(z') - I_n^-(z') &= i \end{aligned} \tag{68}$$

After enforcing the jump condition, we obtain:

$$\begin{bmatrix} [1 + \overrightarrow{\Gamma}_n e^{-j2k_{zn}(z_{n-1}-z')}] & -[1 + \overleftarrow{\Gamma}_n e^{-j2k_{zn}(z'-z_n)}] \\ Y_n[1 - \overrightarrow{\Gamma}_n e^{-j2k_{zn}(z_{n-1}-z')}] & Y_n[1 - \overleftarrow{\Gamma}_n e^{-j2k_{zn}(z'-z_n)}] \end{bmatrix} \begin{bmatrix} V_n^+ \\ V_n^- \end{bmatrix} = \begin{bmatrix} v \\ i \end{bmatrix} \tag{69}$$

Which results in the definitions of V_n^+ and V_n^- in (70).

$$
\begin{aligned}
V_n^+ &= \frac{1}{2D_n}\Big[\big(1-\overleftarrow{\Gamma}_n e^{-j2k_{zn}(z'-z_n)}\big)v+\big(1+\overleftarrow{\Gamma}_n e^{-j2k_{zn}(z'-z_n)}\big)iZ_n\Big]\\
V_n^- &= \frac{1}{2D_n}\Big[\big(1+\overrightarrow{\Gamma}_n e^{-j2k_{zn}(z_{n-1}-z')}\big)iZ_n-\big(1-\overrightarrow{\Gamma}_n e^{-j2k_{zn}(z_{n-1}-z')}\big)v\Big]
\end{aligned}
\tag{70}
$$

Where $D_n = 1-\overleftarrow{\Gamma}_n\overrightarrow{\Gamma}_n e^{-j2\Theta_n}$. One can use the above expressions in (65) and (66) to obtain the complete solutions.

2.1.1 Direct Ray Term Extraction

The above solution is correct, however, the presence of the direct ray (homogeneous medium solution) complicates the evaluation of SIs as discussed earlier. This direct and indirect rays decomposition of the source-excited section is illustrated in Figure 5. For this reason, we extract the direct ray term by setting the reflection coefficients equal to zero, $\overleftarrow{\Gamma}_n = \overrightarrow{\Gamma}_n = 0$ in (70). Hence, we obtain:

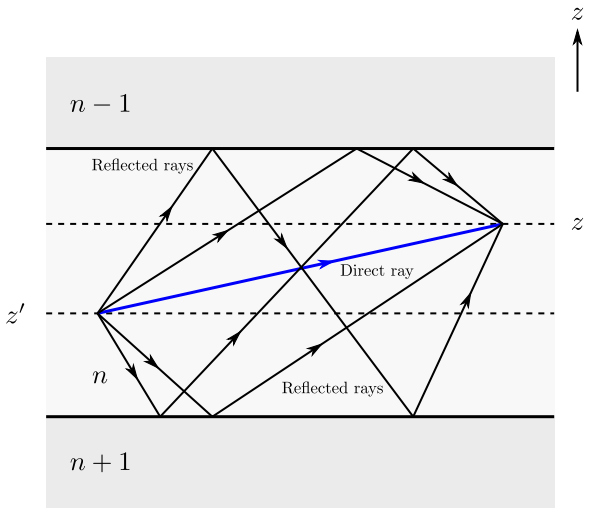

Figure 5: Ray decomposition of the source-excited solution demonstrating direct ray in contrast with the reflected rays.

$$
\begin{aligned}
V_{n0}^+ &= \frac{1}{2}(v+iZ_n)\\
V_{n0}^- &= \frac{1}{2}(iZ_n-v)
\end{aligned}
\tag{71}
$$

As a result, we write the source-excited solutions as follows:

$$V_n(z) = \begin{cases} V_n^+(z) = (V_n^+ - V_{n0}^+)e^{-jk_{zn}(z-z')} + V_n^+ \overrightarrow{\Gamma}' e^{+jk_{zn}(z-z')} & , z > z' \\ V_n^-(z) = (V_n^- - V_{n0}^-)e^{+jk_{zn}(z-z')} + V_n^- \overleftarrow{\Gamma}' e^{-jk_{zn}(z-z')} & , z < z' \end{cases} \tag{72}$$

$$I_n(z) = \begin{cases} I_n^+(z) = Y_n[(V_n^+ - V_{n0}^+)e^{-jk_{zn}(z-z')} - V_n^+ \overrightarrow{\Gamma}' e^{+jk_{zn}(z-z')}] & , z > z' \\ I_n^-(z) = Y_n[(V_{n0}^- - V_n^-)e^{+jk_{zn}(z-z')} + V_n^- \overleftarrow{\Gamma}' e^{-jk_{zn}(z-z')}] & , z < z' \end{cases} \tag{73}$$

In order to account for the subtracted terms, we add the homogeneous medium solution to the DGFs directly which can be expressed in closed forms. The point here is that these terms are nothing but the Sommerfeld identity in (74). Thus, it is meaningless to evaluate this identity numerically each time we compute the fields at some point in the space.

$$\frac{e^{-jkr}}{r} = \int_0^\infty \frac{e^{-jk_z|z|}}{jk_z} J_0(k_\rho \rho) k_\rho dk_\rho \tag{74}$$

2.2 Source-Free Solution $(n \neq m)$

In this type, the solutions in (65) and (66) can be used after substituting $z' = z_{n-1}$ for the case $(n > m)$ and $z' = z_n$ for the case $(n < m)$. The following definitions will be used:

$$\Gamma_{i,j} = \frac{Z_i - Z_j}{Z_i + Z_j} \quad , \quad \tau_{i,j} = 1 + \Gamma_{i,j} = \frac{2Z_i}{Z_i + Z_j} \quad , \quad \Omega_{i,j} = \frac{Z_i Z_j}{Z_i + Z_j} \tag{75}$$

Where $i, j \in [1, N]$ and $i \neq j$.

2.2.1 Down-Looking Case $(n > m)$

The following solution is considered:

$$\begin{aligned} V_n(z) &= V_n^- e^{-j\Theta_n}[e^{jk_{zn}(z-z_n)} + \overleftarrow{\Gamma}_n e^{-jk_{zn}(z-z_n)}] \\ -Z_n I_n(z) &= V_n^- e^{-j\Theta_n}[e^{jk_{zn}(z-z_n)} - \overleftarrow{\Gamma}_n e^{-jk_{zn}(z-z_n)}] \end{aligned} \tag{76}$$

Here, it is possible to express the solutions as follows:

$$\begin{bmatrix} V_n(z) \\ I_n(z) \end{bmatrix} = \begin{bmatrix} 1 & 1 \\ -Y_n & Y_n \end{bmatrix} \begin{bmatrix} e^{jk_{zn}(z-z_n)} & 0 \\ 0 & e^{-jk_{zn}(z-z_n)} \end{bmatrix} \begin{bmatrix} 1 \\ \overleftarrow{\Gamma}_n \end{bmatrix} e^{-j\Theta_n} V_n^- \tag{77}$$

One can use the boundary condition in (63) as follows:

$$\begin{bmatrix} V_{n+1}(z_n) \\ I_{n+1}(z_n) \end{bmatrix} = \begin{bmatrix} 1 & 0 \\ \sigma_n^s & 1 \end{bmatrix} \begin{bmatrix} V_n(z_n) \\ I_n(z_n) \end{bmatrix} \tag{78}$$

After re-arranging the matrices, we can obtain the system:

$$\begin{bmatrix} 1 \\ \overleftarrow{\Gamma}_{n+1} e^{-j2\Theta_{n+1}} \end{bmatrix} V_{n+1}^- = \tau_{n,n+1}^{-1} \begin{bmatrix} M_{11,n} & M_{12,n} \\ M_{21,n} & M_{22,n} \end{bmatrix} \begin{bmatrix} 1 \\ \overleftarrow{\Gamma}_n \end{bmatrix} e^{-j\Theta_n} V_n^- \tag{79}$$

Where

$$\begin{aligned} M_{11,n} &= 1 - \Omega_{n,n+1}\sigma_n^s \\ M_{12,n} &= \Gamma_{n,n+1} - \Omega_{n,n+1}\sigma_n^s \\ M_{21,n} &= \Gamma_{n,n+1} + \Omega_{n,n+1}\sigma_n^s \\ M_{22,n} &= 1 + \Omega_{n,n+1}\sigma_n^s \end{aligned} \tag{80}$$

Thus, we obtain the relation:

$$V_{n+1}^- = \frac{(1 + \overleftarrow{\Gamma}_n) e^{-j\Theta_n}}{1 + \overleftarrow{\Gamma}_{n+1} e^{-j2\Theta_{n+1}}} V_n^- = \overleftarrow{\tau}_n V_n^- \tag{81}$$

For computing V_n^-, we start from $n = m + 1$ and compute:

$$V_n^- = \frac{V_m(z_m)}{1 + \overleftarrow{\Gamma}_n e^{-j2\Theta_n}} = \frac{(1 + \overleftarrow{\Gamma}_m) e^{-jk_{zm}(z' - z_m)}}{1 + \overleftarrow{\Gamma}_n e^{-j2\Theta_n}} V_m^- \tag{82}$$

Where, V_m^- from (70). Then, we use the relation in (82) to compute $V_{m+2}^-, \ldots, V_n^-$ downward. The overall transmission coefficient $\overleftarrow{\tau} = \prod_{n=1}^{N-1} \overleftarrow{\tau}_n$. Also, the recursive reflection coefficient relation is:

$$\overleftarrow{\Gamma}_n = \frac{[\Gamma_{n+1,n} - \Omega_{n+1,n}\sigma_n^s] + [1 - \Omega_{n+1,n}\sigma_n^s] \overleftarrow{\Gamma}_{n+1} e^{-j2\Theta_{n+1}}}{[1 + \Omega_{n+1,n}\sigma_n^s] + [\Gamma_{n+1,n} + \Omega_{n+1,n}\sigma_n^s] \overleftarrow{\Gamma}_{n+1} e^{-j2\Theta_{n+1}}} \tag{83}$$

For computing the reflection coefficient $\overleftarrow{\Gamma}_n$, we start from $\overleftarrow{\Gamma}_N$ and compute $\overleftarrow{\Gamma}_{N-1}, \ldots, \overleftarrow{\Gamma}_n$ upward. In addition to the above, one can compute the basic reflectivity, transmissivity, and absorptivity expressions, $|\overleftarrow{R}|^2$, $|\overleftarrow{T}|^2$, and $|\overleftarrow{A}|^2$, respectively.

$$
\begin{aligned}
|\overleftarrow{R}|^2 &= |\overleftarrow{\Gamma}|^2 \\
|\overleftarrow{T}|^2 &= \mathrm{Re}\Big[\frac{Z_1}{Z_N}\Big]|\overleftarrow{\tau}|^2 \\
|\overleftarrow{A}|^2 &= 1 - |\overleftarrow{R}|^2 - |\overleftarrow{T}|^2
\end{aligned}
\tag{84}
$$

2.2.2 Up-Looking Case ($n < m$)

The following solution is considered:

$$
\begin{aligned}
V_n(z) &= V_n^+ e^{-j\Theta_n}[e^{-jk_{zn}(z-z_{n-1})} + \overrightarrow{\Gamma}_n e^{jk_{zn}(z-z_{n-1})}] \\
Z_n I_n(z) &= V_n^+ e^{-j\Theta_n}[e^{-jk_{zn}(z-z_{n-1})} - \overrightarrow{\Gamma}_n e^{jk_{zn}(z-z_{n-1})}]
\end{aligned}
\tag{85}
$$

Here, it is possible to express the solutions as follows:

$$
\begin{bmatrix} V_n(z) \\ I_n(z) \end{bmatrix} = \begin{bmatrix} 1 & 1 \\ Y_n & -Y_n \end{bmatrix} \begin{bmatrix} e^{-jk_{zn}(z-z_{n-1})} & 0 \\ 0 & e^{jk_{zn}(z-z_{n-1})} \end{bmatrix} \begin{bmatrix} 1 \\ \overrightarrow{\Gamma}_n \end{bmatrix} e^{-j\Theta_n} V_n^+ \tag{86}
$$

One can use the boundary condition in (64) as follows:

$$
\begin{bmatrix} V_{n-1}(z_{n-1}) \\ I_{n-1}(z_{n-1}) \end{bmatrix} = \begin{bmatrix} 1 & 0 \\ -\sigma_{n-1}^s & 1 \end{bmatrix} \begin{bmatrix} V_n(z_{n-1}) \\ I_n(z_{n-1}) \end{bmatrix} \tag{87}
$$

After re-arranging the matrices, we can obtain the system:

$$
\begin{bmatrix} 1 \\ \overrightarrow{\Gamma}_{n-1} e^{-j2\Theta_{n-1}} \end{bmatrix} V_{n-1}^+ = \tau_{n,n-1}^{-1} \begin{bmatrix} M_{11,n} & M_{12,n} \\ M_{21,n} & M_{22,n} \end{bmatrix} \begin{bmatrix} 1 \\ \overrightarrow{\Gamma}_n \end{bmatrix} e^{-j\Theta_n} V_n^+ \tag{88}
$$

Where

$$
\begin{aligned}
M_{11,n} &= 1 - \Omega_{n,n-1}\sigma_{n-1}^s \\
M_{12,n} &= \Gamma_{n,n-1} - \Omega_{n,n-1}\sigma_{n-1}^s \\
M_{21,n} &= \Gamma_{n,n-1} + \Omega_{n,n-1}\sigma_{n-1}^s \\
M_{22,n} &= 1 + \Omega_{n,n-1}\sigma_{n-1}^s
\end{aligned}
\tag{89}
$$

Thus, we obtain the relation:

$$
V_{n-1}^+ = \frac{(1 + \overrightarrow{\Gamma}_n)e^{-j\Theta_n}}{1 + \overrightarrow{\Gamma}_{n-1} e^{-j2\Theta_{n-1}}} V_n^+ = \overrightarrow{\tau}_n V_n^+ \tag{90}
$$

For computing V_n^+, we start from $n = m-1$ and compute:

$$V_n^+ = \frac{V_m(z_{m-1})}{1+\overrightarrow{\Gamma}_n e^{-j2\Theta_n}} = \frac{(1+\overrightarrow{\Gamma}_m)e^{-jk_{zm}(z_{m-1}-z')}}{1+\overrightarrow{\Gamma}_n e^{-j2\Theta_n}} V_m^+ \tag{91}$$

Where, V_m^+ from (70). Then, we use the relation in (91) to compute $V_{m-2}^+, \ldots, V_n^+$ upward. The overall transmission coefficient $\overrightarrow{\tau} = \prod_{n=2}^{N} \overrightarrow{\tau}_n$. Also, the recursive reflection coefficient relation is:

$$\overrightarrow{\Gamma}_n = \frac{[\Gamma_{n-1,n} - \Omega_{n-1,n}\sigma_{n-1}^s] + [1-\Omega_{n-1,n}\sigma_{n-1}^s]\overrightarrow{\Gamma}_{n-1} e^{-j2\Theta_{n-1}}}{[1+\Omega_{n-1,n}\sigma_{n-1}^s] + [\Gamma_{n-1,n} + \Omega_{n-1,n}\sigma_{n-1}^s]\overrightarrow{\Gamma}_{n-1} e^{-j2\Theta_{n-1}}} \tag{92}$$

For computing the reflection coefficient $\overrightarrow{\Gamma}_n$, we start from $\overrightarrow{\Gamma}_1$ and compute $\overrightarrow{\Gamma}_2, \ldots, \overrightarrow{\Gamma}_n$ downward. In addition to the above, one can compute the basic reflectivity, transmissivity, and absorptivity expressions, $|\overrightarrow{R}|^2$, $|\overrightarrow{T}|^2$, and $|\overrightarrow{A}|^2$, respectively.

$$\begin{aligned} |\overrightarrow{R}|^2 &= |\overrightarrow{\Gamma}|^2 \\ |\overrightarrow{T}|^2 &= \mathrm{Re}\Big[\frac{Z_N}{Z_1}\Big]|\overrightarrow{\tau}|^2 \\ |\overrightarrow{A}|^2 &= 1 - |\overrightarrow{R}|^2 - |\overrightarrow{T}|^2 \end{aligned} \tag{93}$$

3 Fields Evaluation

In section, we will discuss the evaluation of fields due to various types of sources and excitations

3.1 Dyadic Green's Functions

The first type of fields to be evaluated is due to a point source. Here, we would like to demonstrate how to compute the expressions in (26)-(61). This is done by using the solutions of the TLGFs as described in the previous section and then we numerically evaluate the SIs as in (22). It is important here to introduce the definition of ($\sqrt{\ }$) of k_z in the complex k_ρ domain illustrated in Figure 6. This definition results in four Riemann sheets as shown in Figure 7. Note that only k_{z1} and k_{zN} matters in this description as seen from the reflection coefficients. When evaluating the spatial domain DGFs, we choose the definition on Riemann sheet I (*i.e.*, $\mathrm{Im}[k_{z1}] < 0$ and $\mathrm{Im}[k_{N1}] < 0$).

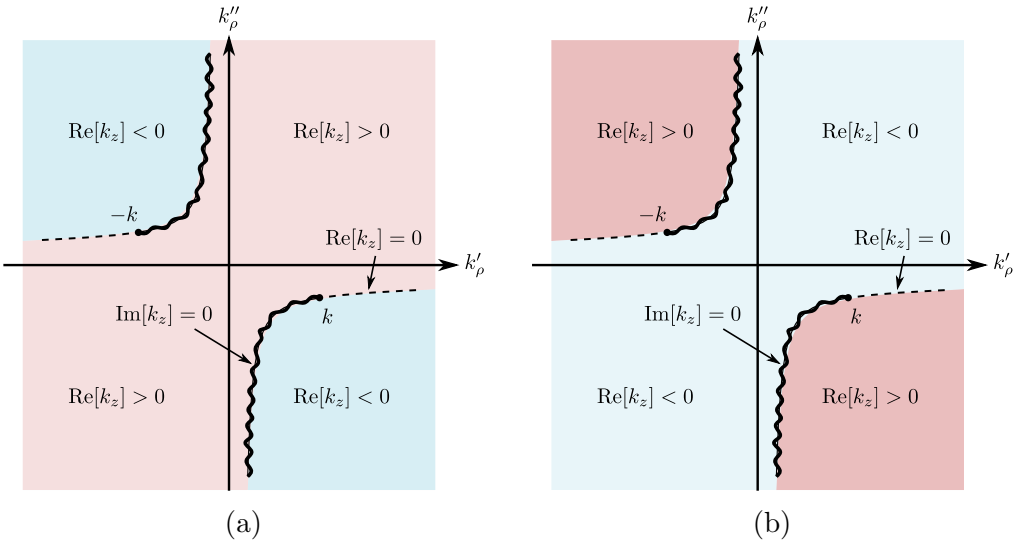

Figure 6: Definition of $k_z = \sqrt{k^2 - k_\rho^2}$ on Riemann sheets. (a) Proper sheet I ($\mathrm{Im}[k_z] < 0$) (b) Improper sheet II ($\mathrm{Im}[k_z] > 0$).

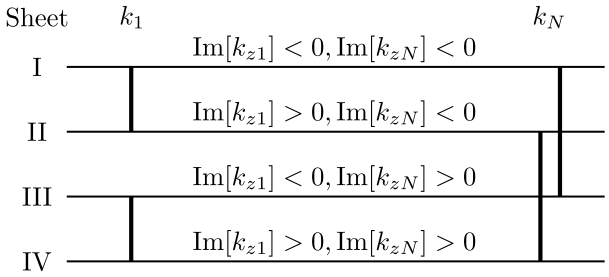

Figure 7: Definitions of the four Riemann sheets associated with layered media spectral DGFs.

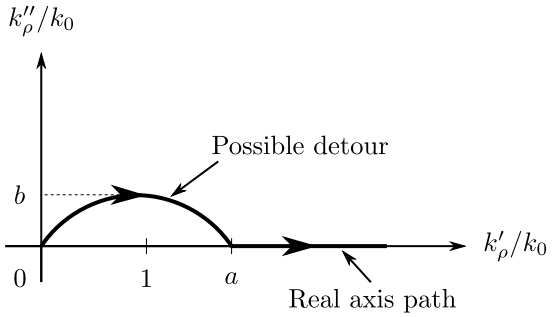

Figure 8: The real axis integral defined with a detour into the first quadrant for I_a.

The SIs can written as in (94) using the real axis integration as in Figure 8. Here, the integrals can be divided into two parts as follows:

$$I = \int_0^\infty \tilde{G}(k_\rho; z|z') J_n(k_\rho \rho) k_\rho dk_\rho = \left(\int_0^a + \int_a^\infty \right) \tilde{G}(k_\rho; z|z') J_n(k_\rho \rho) k_\rho dk_\rho \tag{94}$$

Where $a = k_0[\max(\sqrt{\mu_n \epsilon_n})+1]$. Those are typical choices for this integral. Since $\tilde{G}(k_\rho; z|z')$ has a singularity at branch points $k_\rho = k_1$ and $k_\rho = k_N$. Thus, we have to indent the integration path as shown in Figure 8. The detour can be parameterized using the real variable t as follows:

$$\begin{aligned} k_\rho &= t + jb \sin(\frac{\pi t}{a}) \\ dk_\rho &= \left(1 + j\frac{\pi b}{a} \cos(\frac{\pi t}{a})\right) dt \end{aligned} \tag{95}$$

Where t takes the real values $0 \leq t \leq a$. For $k_\rho > a$, we simply return to the real axis with $k_\rho = t$. Also,

$$b = \begin{cases} \min(k_0, \frac{1}{\rho}) & , \rho > |z - z'| \\ k_0 & , \text{otherwise} \end{cases} \tag{96}$$

Also, we recommend $b = 0.001k_0$ when $\sqrt{\rho^2 + |z - z'|^2} > 20\lambda_0$. If the point of interest is much greater than this, we prefer to switch into the far-field approximation as discussed later. In addition to this, we provide an example of the integrands before and after applying this detour in Figure 9. The frequency of these ripples increase with ρ which adds more difficulties to the numerical evaluation of these integrals. The example shown in Figure 9 represents the worst case scenario when $z = z'$.

Here, it is important to focus on the advantage of extracting the singular direct ray term from the TLGFs. When the direct ray is removed, the infinite integrands become finite in k_ρ and magnitude as seen in Figure 10. This makes any suitable quadrature rule applicable to evaluate the integrals numerically and only need to compute $I = \int_0^a \tilde{G}(k_\rho; z|z') J_n(k_\rho \rho) k_\rho dk_\rho$ instead. The homogeneous media DGFs for all field and source types can be easily obtained from Maxwell's equations. We can adopt the notation $x_1 = x$, $x_2 = y$ and $x_3 = z$. Hence, for $i, j = 1, 2, 3$, the direct ray DGFs can be written in a compact form as follows:

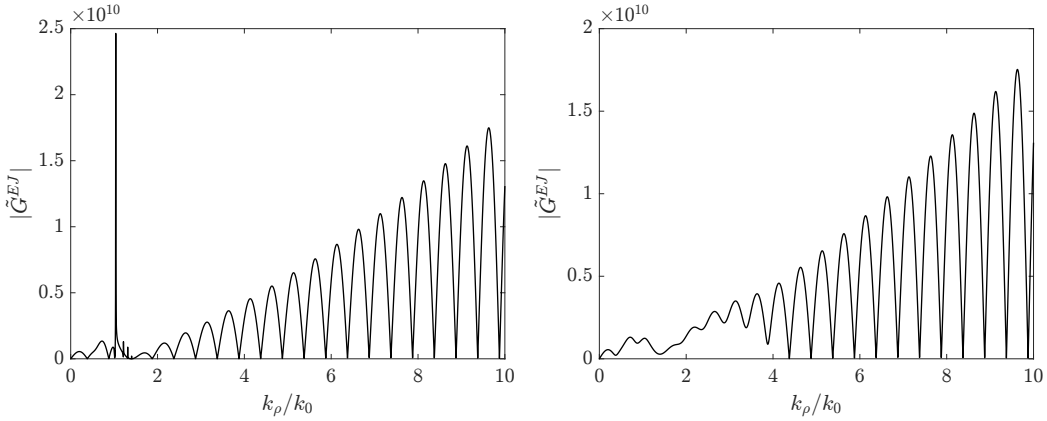

(a) (b)

Figure 9: An example of the DGFs integrands behavior vs k_ρ when $z = z'$. The growing ripples are caused by the inclusion of the direct ray term in the TLGFs solutions. (a) Without detour (b) After detour.

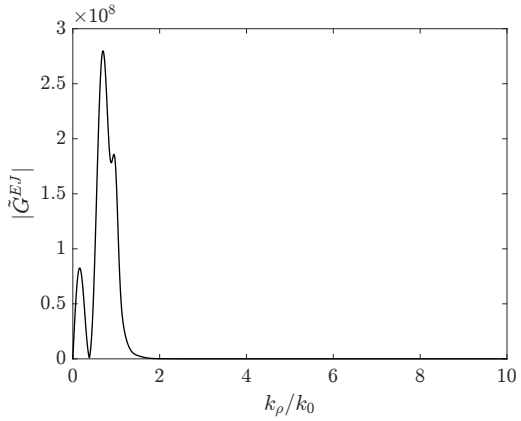

Figure 10: An example of the DGFs integrands behavior vs k_ρ when $z = z'$ after applying the recommended detour and extracting the direct ray term from the TLGFs solutions.

$$
\begin{aligned}
G^{EJ}_{x_i x_j} &= -j\omega\mu_0\mu'\left[g\delta_{ij} + \frac{1}{k^2}\left[\frac{1}{R}\frac{\partial g}{\partial R}\delta_{ij} + \frac{x_i - x'_i}{R}\frac{x_j - x'_j}{R}\left(\frac{\partial^2 g}{\partial R^2} - \frac{1}{R}\frac{\partial g}{\partial R}\right)\right]\right] \\
G^{HJ}_{x_i x_j} &= \frac{x'_k - x_k}{R}\frac{\partial g}{\partial R}\epsilon_{ijk} \\
G^{EM}_{x_i x_j} &= \frac{x_k - x'_k}{R}\frac{\partial g}{\partial R}\epsilon_{ijk} \\
G^{HM}_{x_i x_j} &= -j\omega\epsilon_0\epsilon'\left[g\delta_{ij} + \frac{1}{k^2}\left[\frac{1}{R}\frac{\partial g}{\partial R}\delta_{ij} + \frac{x_i - x'_i}{R}\frac{x_j - x'_j}{R}\left(\frac{\partial^2 g}{\partial R^2} - \frac{1}{R}\frac{\partial g}{\partial R}\right)\right]\right]
\end{aligned} \tag{97}
$$

Where:

$$
\begin{aligned}
g(\boldsymbol{r}|\boldsymbol{r}') &= \frac{e^{-jkR}}{4\pi R} \\
\frac{\partial g(\boldsymbol{r}|\boldsymbol{r}')}{\partial R} &= -\frac{(1+jkR)}{R}g(\boldsymbol{r}|\boldsymbol{r}') \\
\frac{\partial^2 g(\boldsymbol{r}|\boldsymbol{r}')}{\partial R^2} &= -\frac{(1+jkR)}{R}\frac{\partial g(\boldsymbol{r}|\boldsymbol{r}')}{\partial R} + \frac{g(\boldsymbol{r}|\boldsymbol{r}')}{R^2}
\end{aligned} \tag{98}
$$

Where $R = |\boldsymbol{r} - \boldsymbol{r}'| \neq 0$. The δ_{ij} and ϵ_{ijk} are the Kronecker and Levi-Civita permutation symbols respectively and defined as:

$$
\delta_{ij} = \begin{cases} 1 & , i = j \\ 0 & , i \neq j \end{cases} \tag{99}
$$

$$
\epsilon_{ijk} = \begin{cases} +1 & , ijk = 123 \quad 231 \quad 312 \\ -1 & , ijk = 132 \quad 213 \quad 321 \\ 0 & , \text{otherwise} \end{cases} \tag{100}
$$

Note that when $R \longrightarrow 0$, we substitute the following values for direct ray DGFs at the singularity:

$$
\begin{aligned}
\lim_{R\to 0} G^{EJ}_{x_i x_j} &= \frac{j}{3\omega\epsilon_0\epsilon'}\delta_{ij} \\
\lim_{R\to 0} G^{HJ}_{x_i x_j} &= 0 \\
\lim_{R\to 0} G^{EM}_{x_i x_j} &= 0 \\
\lim_{R\to 0} G^{HM}_{x_i x_j} &= \frac{j}{3\omega\mu_0\mu'}\delta_{ij}
\end{aligned} \tag{101}
$$

Thus, after computing (26)-(61) without the direct ray term, we add the solutions from (97) when $n = m$ and ignore this step when $n \neq m$.

3.2 Plane Wave Excitation

The evaluation of the plane wave excitation in planar layered media is a very important. An illustration of the wavevector of an incident plane wave from the top layer is shown in Figure 11. The plane wave is decomposed into two components E^i_θ and E^i_φ allowing the definition of TE and TM polarizations, respectively.

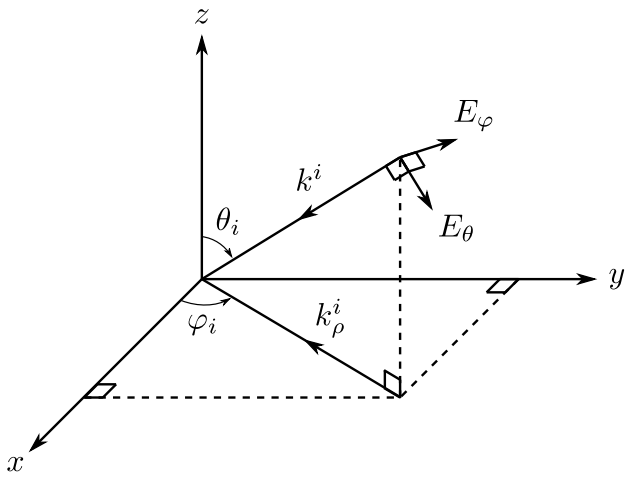

Figure 11: Schematic of the incident plane wave excitation from the top layer. The wave vector $\boldsymbol{k}^i$ is defined by the incidence angles (θ_i, φ_i).

The analysis of plane wave excitation can be simplified by using the surface equivalence theorem. Thus, it is possible to define an equivalent magnetic surface current at z_0 as $\boldsymbol{E} \times \hat{\boldsymbol{n}} = \boldsymbol{M}_s$.[1] Using image theorem, the problem in the range $z_N \leq z \leq z_0$ can be solved using magnetic currents sheet $\boldsymbol{M}_s = 2\hat{\boldsymbol{z}} \times \boldsymbol{E}^i \delta(z - z_0)$. Also, the transverse wavenumber is $k^i_\rho = k_1 \sin(\theta_i)$. The incident field in $z > z_0$ is expressed in (102).

$$\boldsymbol{E}^i = \boldsymbol{E}_0 e^{j\boldsymbol{k}^i_\rho \cdot \boldsymbol{\rho}} e^{jk_1 \cos(\theta_i) z} \tag{102}$$

Where $\boldsymbol{E}_0$ is given as:

$$\boldsymbol{E}_0 = E^i_\theta \hat{\boldsymbol{\theta}}_i + E^i_\varphi \hat{\boldsymbol{\varphi}}_i \tag{103}$$

[1] Notice that $\hat{\boldsymbol{n}} = -\hat{\boldsymbol{z}}$.

According to this choice, for TM excitation we set $E^i_\varphi = 0$, while and for TE excitation we set $E^i_\theta = 0$. The evaluation of the fields due to this excitation can be simplified by exploiting Fourier transform properties. Hence, the evaluation is performed in the spectral domain where $\hat{\boldsymbol{\rho}}_i = \hat{\boldsymbol{u}}$ and $\hat{\boldsymbol{\varphi}}_i = \hat{\boldsymbol{v}}$. Thus, the spectral domain equivalent current $\tilde{\boldsymbol{M}}_s$ is given in (104).

$$\tilde{\boldsymbol{M}}_s = 2\big[E^i_\theta \cos(\theta_i)\hat{\boldsymbol{v}} - E^i_\varphi \hat{\boldsymbol{u}}\big] e^{jk_1 \cos(\theta_i) z_0} (2\pi)^2 \delta(\boldsymbol{k}_\rho + \boldsymbol{k}^i_\rho)\delta(z - z_0) \tag{104}$$

Now, the convolution integrals in (104) are used to evaluate the fields in the range of interest $z_N \leq z \leq z_0$ as in (105). Note that these convolutions reduce into dot product because of $\delta(z - z_0)$.

$$\begin{aligned} \tilde{\boldsymbol{E}} &= \langle \underline{\tilde{\boldsymbol{G}}}^{EM}; \tilde{\boldsymbol{M}}_s \rangle \\ \tilde{\boldsymbol{H}} &= \langle \underline{\tilde{\boldsymbol{G}}}^{HM}; \tilde{\boldsymbol{M}}_s \rangle \end{aligned} \tag{105}$$

Upon applying the inverse Fourier transform to the resulting fields, this reduces to the expressions in (106). Where the definitions $Z^e_1 = \eta_1 \cos(\theta_i)$ and $Z^h_1 = \eta_1 / \cos(\theta_i)$ were used.

$$\begin{aligned} \boldsymbol{E} &= -2\boldsymbol{E}_0 \cdot \big[V^e_v \cos(\theta_i)\hat{\boldsymbol{\theta}}_i\hat{\boldsymbol{\rho}}_i + V^h_v \hat{\boldsymbol{\varphi}}_i\hat{\boldsymbol{\varphi}}_i - I^e_v Z^e_1 \frac{\epsilon_1}{\epsilon} \sin(\theta_i)\hat{\boldsymbol{\theta}}_i\hat{\boldsymbol{z}}\big] e^{j\boldsymbol{k}^i_\rho \cdot \boldsymbol{\rho}} e^{jk_1 \cos(\theta_i) z_0} \\ \boldsymbol{H} &= -2\boldsymbol{E}_0 \cdot \big[I^e_v \cos(\theta_i)\hat{\boldsymbol{\theta}}_i\hat{\boldsymbol{\varphi}}_i - I^h_v \hat{\boldsymbol{\varphi}}_i\hat{\boldsymbol{\rho}}_i + V^h_v \frac{1}{Z^h_1} \frac{\mu_1}{\mu} \sin(\theta_i)\hat{\boldsymbol{\varphi}}_i\hat{\boldsymbol{z}}\big] e^{j\boldsymbol{k}^i_\rho \cdot \boldsymbol{\rho}} e^{jk_1 \cos(\theta_i) z_0} \end{aligned} \tag{106}$$

3.3 Far-Fields Computation

The far-field due to a point source can be evaluated using the equivalence theorem combined with image theorem in a similar way to the plane wave excitation fields. Here, the interest is in the top and bottom layers. Hence, the solution will be considered for $z > z_0$ and $z < z_N$. The solution for $z < z_N$ can be easily obtained using a similar procedure to the one used for $z > z_0$. The electric field due to equivalent magnetic current at $z = z_0$ is shown in (107) using free-space Green's function.

$$\boldsymbol{E} = -\nabla \times \iiint \frac{e^{-jk_1|\boldsymbol{r} - \boldsymbol{r}'|}}{4\pi|\boldsymbol{r} - \boldsymbol{r}'|} \boldsymbol{M}(\boldsymbol{r}')d\boldsymbol{r}' \tag{107}$$

In the far-field, it is possible to make the following approximations $\nabla \sim -jk\hat{\boldsymbol{r}}$ and $|\boldsymbol{r} - \boldsymbol{r}'| \sim r - \boldsymbol{r}' \cdot \hat{\boldsymbol{r}}$. Applying these asymptotic expressions to

(107), this results in equation (108). Here, $k_1\boldsymbol{r}'\cdot\hat{\boldsymbol{r}} = k_1(\boldsymbol{\rho}'+z'\hat{\boldsymbol{z}})\cdot\hat{\boldsymbol{r}} = \boldsymbol{k}_\rho\cdot\boldsymbol{\rho}' + k_1\cos(\theta)z'$. Also, $\boldsymbol{k}_\rho = k_1\sin(\theta)\hat{\boldsymbol{\rho}}$.

$$\begin{aligned}\boldsymbol{E} &\sim jk_1\frac{e^{-jk_1r}}{4\pi r}\int_{-\infty}^{\infty}\int_{-\infty}^{\infty}\int_{-\infty}^{\infty}\hat{\boldsymbol{r}}\times\boldsymbol{M}(\boldsymbol{r}')\delta(z'-z_0)e^{j\boldsymbol{k}_\rho\cdot\boldsymbol{\rho}'}e^{jk_1\cos(\theta)z'}d\boldsymbol{\rho}'dz' \\ &\sim jk_1\frac{e^{-jk_1r}}{4\pi r}e^{jk_1\cos(\theta)z_0}\left[\hat{\boldsymbol{r}}\times\tilde{\boldsymbol{M}}_s(\boldsymbol{k}_\rho;z_0)\right]\end{aligned} \tag{108}$$

Considering the magnetic currents sheet $\boldsymbol{M}_s = 2\hat{\boldsymbol{z}}\times\boldsymbol{E}\delta(z-z_0)$, the spectral electric field can be found using (105). For electric dipole k_J:

$$\tilde{\boldsymbol{J}} = \mathcal{F}\{I\boldsymbol{l}_{k_J}\delta(\boldsymbol{\rho}-\boldsymbol{\rho}_{k_J})\delta(z-z_{k_J})\} = I\boldsymbol{l}_{k_J}e^{j\boldsymbol{k}_\rho\cdot\boldsymbol{\rho}_{k_J}}\delta(z-z_{k_J}) \tag{109}$$

Thus, the far field for $z>z_0$ can be found using (110).

$$\boldsymbol{E} \sim -jk_1\frac{e^{-jk_1r}}{2\pi r}e^{jk_1\cos(\theta)z_0}\left[\hat{\boldsymbol{r}}\times\hat{\boldsymbol{z}}\times\underline{\tilde{\boldsymbol{G}}}^{EJ}(\boldsymbol{k}_\rho;z_0|z_{k_J})\right]\cdot I\boldsymbol{l}_{k_J}e^{j\boldsymbol{k}_\rho\cdot\boldsymbol{\rho}_{k_J}} \tag{110}$$

For the electric and magnetic dipoles k_J and k_M, respectively, it is possible to write the far-field due to these dipoles for $z>z_0$ in (111) and (112). Where, the far field for $z<z_N$ is in (113) and (114).

For $z>z_0$, we substitute $k_\rho = k_1\sin(\theta)$, and this corresponds to $0\le\theta\le\pi/2$:

$$\begin{aligned}\boldsymbol{E} \sim -jk_1\frac{e^{-jk_1r}}{2\pi r}e^{jk_1\cos(\theta)z_0}\big[&V_i^e\hat{\boldsymbol{\theta}}\hat{\boldsymbol{\rho}}+V_i^h\cos(\theta)\hat{\boldsymbol{\varphi}}\hat{\boldsymbol{\varphi}} \\ &- V_v^e\eta_1\frac{\epsilon_1}{\epsilon'}\sin(\theta)\hat{\boldsymbol{\theta}}\hat{\boldsymbol{z}}\big]\cdot I\boldsymbol{l}_{k_J}e^{j\boldsymbol{k}_\rho\cdot\boldsymbol{\rho}_{k_J}}\end{aligned} \tag{111}$$

$$\begin{aligned}\boldsymbol{E} \sim jk_1\frac{e^{-jk_1r}}{2\pi r}e^{jk_1\cos(\theta)z_0}\big[&V_v^h\cos(\theta)\hat{\boldsymbol{\varphi}}\hat{\boldsymbol{\rho}}-V_v^h\hat{\boldsymbol{\theta}}\hat{\boldsymbol{\varphi}} \\ &- V_i^h\frac{1}{\eta_1}\frac{\mu_1}{\mu'}\cos(\theta)\hat{\boldsymbol{\varphi}}\hat{\boldsymbol{z}}\big]\cdot K\boldsymbol{l}_{k_M}e^{j\boldsymbol{k}_\rho\cdot\boldsymbol{\rho}_{k_M}}\end{aligned} \tag{112}$$

For $z<z_N$, we substitute $k_\rho = k_N\sin(\theta)$, and this corresponds to $\pi/2\le\theta\le\pi$:

$$\boldsymbol{E} \sim -jk_N \frac{e^{-jk_N r}}{2\pi r} e^{-jk_N \cos(\theta) z_N} \big[V_i^e \hat{\boldsymbol{\theta}}\hat{\boldsymbol{\rho}} + V_i^h \cos(\theta)\hat{\boldsymbol{\varphi}}\hat{\boldsymbol{\varphi}} - V_v^e \eta_N \frac{\epsilon_N}{\epsilon'} \sin(\theta)\hat{\boldsymbol{\theta}}\hat{\boldsymbol{z}} \big] \cdot I\boldsymbol{l}_{k_J} e^{j\boldsymbol{k}_\rho \cdot \boldsymbol{\rho}_{k_J}} \tag{113}$$

$$\boldsymbol{E} \sim jk_N \frac{e^{-jk_N r}}{2\pi r} e^{jk_N \cos(\theta) z_N} \big[V_v^h \cos(\theta)\hat{\boldsymbol{\varphi}}\hat{\boldsymbol{\rho}} - V_v^h \hat{\boldsymbol{\theta}}\hat{\boldsymbol{\varphi}} - V_i^h \frac{1}{\eta_N} \frac{\mu_N}{\mu'} \cos(\theta)\hat{\boldsymbol{\varphi}}\hat{\boldsymbol{z}} \big] \cdot K\boldsymbol{l}_{k_M} e^{j\boldsymbol{k}_\rho \cdot \boldsymbol{\rho}_{k_M}} \tag{114}$$

4 Modal Analysis

In this section we discuss the modal analysis. One can seek spatial fields solutions with $e^{-j\boldsymbol{k}_\rho \cdot \boldsymbol{\rho}}$ dependency ($\boldsymbol{k}_\rho$ is a fixed eigenvalue) which corresponds to $\delta(\boldsymbol{k}_\rho)$ shifted by the eigenvalue in the spectral domain and reduces the source-free expressions from (14). This leads to two possible e and h or TM and TE modes, respectively, as in (115) and (116). Hence, it is possible to study the modal analysis for planar layered media using the TL quantities directly, (*i.e.*, the modal fields are voltages and currents solutions of the TL).

$$\boldsymbol{E}_t^e = V^e \hat{\boldsymbol{u}} \quad , \quad \boldsymbol{H}_t^e = I^e \hat{\boldsymbol{v}} \quad , \quad E_z^e = -\frac{k_\rho}{k_0} \frac{\eta_0 I^e}{\epsilon} \tag{115}$$

$$\boldsymbol{E}_t^h = V^h \hat{\boldsymbol{v}} \quad , \quad \boldsymbol{H}_t^h = -I^h \hat{\boldsymbol{u}} \quad , \quad H_z^h = \frac{k_\rho}{k_0} \frac{V^h}{\eta_0 \mu} \tag{116}$$

Here, we seek to derive a Dispersion Function (DF) when set to zero results in an eigenvalue equation. The eigenvalues are the resonance modes in this structure. Also, we will drop the mode type for simplicity.

4.1 T-Matrix Formulation

The source-free section n solution can be written as in (117).

$$\begin{aligned} V_n(z) &= V_n^+ e^{-jk_{zn}(z-z_n)} + V_n^- e^{jk_{zn}(z-z_n)} \\ I_n(z) &= Y_n \big[V_n^+ e^{-jk_{zn}(z-z_n)} - V_n^- e^{jk_{zn}(z-z_n)} \big] \end{aligned} \tag{117}$$

The boundary conditions between sections n and $n-1$ at $z = z_{n-1}$ must be enforced in order to construct the basic T-matrix relation. From (64), it is possible to re-arrange the expressions in a convenient matrix form at the boundary z_{n-1}. This results in the expression in (118) and (119).

$$\begin{bmatrix} V_n(z_{n-1}) \\ I_n(z_{n-1}) \end{bmatrix} = \begin{bmatrix} 1 & 1 \\ Y_n & -Y_n \end{bmatrix} \begin{bmatrix} e^{-j\Theta_n} & 0 \\ 0 & e^{j\Theta_n} \end{bmatrix} \begin{bmatrix} V_n^+ \\ V_n^- \end{bmatrix} \tag{118}$$

$$\begin{bmatrix} V_{n-1}(z_{n-1}) \\ I_{n-1}(z_{n-1}) \end{bmatrix} = \begin{bmatrix} 1 & 1 \\ Y_{n-1} & -Y_{n-1} \end{bmatrix} \begin{bmatrix} V_{n-1}^+ \\ V_{n-1}^- \end{bmatrix} \tag{119}$$

Now, it is possible to form the matrix relation in (120) between incident V^+ and reflected V^- voltages in sections n and $n-1$. This results in the matrix $\big[\boldsymbol{T}_n\big]$ which is the T-matrix relating sections n and $n-1$. $\big[\boldsymbol{T}_n\big]$ will become the building block for the final DF.

$$\begin{bmatrix} V_n^+ \\ V_n^- \end{bmatrix} = \big[T_n\big] \begin{bmatrix} V_{n-1}^+ \\ V_{n-1}^- \end{bmatrix} \tag{120}$$

The elements of matrix $\big[\boldsymbol{T}_n\big]$ can be expressed as follows:

$$\big[\boldsymbol{T}_n\big] = \begin{bmatrix} T_{11,n} & T_{12,n} \\ T_{21,n} & T_{22,n} \end{bmatrix} \tag{121}$$

Where,

$$\begin{aligned} T_{11,n} &= \frac{1}{2}\Big[1 + Q_n + Z_n\sigma_{n-1}^s\Big]e^{j\Theta_n} \\ T_{12,n} &= \frac{1}{2}\Big[1 - Q_n + Z_n\sigma_{n-1}^s\Big]e^{j\Theta_n} \\ T_{21,n} &= \frac{1}{2}\Big[1 - Q_n - Z_n\sigma_{n-1}^s\Big]e^{-j\Theta_n} \\ T_{22,n} &= \frac{1}{2}\Big[1 + Q_n - Z_n\sigma_{n-1}^s\Big]e^{-j\Theta_n} \end{aligned} \tag{122}$$

Where $Q_n = Z_n/Z_{n-1}$. The overall T-matrix can be defined in (123) by equation the contiguous sections.

$$\begin{bmatrix} V_N^+ \\ V_N^- \end{bmatrix} = \underbrace{\big[\boldsymbol{T}_N\big]\ldots\big[\boldsymbol{T}_2\big]}_{\big[\boldsymbol{T}\big]} \begin{bmatrix} V_1^+ \\ V_1^- \end{bmatrix} \tag{123}$$

The boundary impedances $\overleftarrow{Z}_N$ and $\overrightarrow{Z}_1$ will be used to represent the all possible terminations. Thus, the following relations are used to introduce these terminations in the dispersion relation:

$$\begin{bmatrix} 1 & \overleftarrow{Z}_N \end{bmatrix} \begin{bmatrix} V_N(z_N) \\ I_N(z_N) \end{bmatrix} = 0 \tag{124}$$

$$\begin{bmatrix} V_1(z_0) \\ I_1(z_0) \end{bmatrix} = \begin{bmatrix} \overrightarrow{Z}_1 \\ 1 \end{bmatrix} I_1(z_0) \tag{125}$$

Also,

$$\begin{bmatrix} V_1^+ \\ V_1^- \end{bmatrix} = \frac{1}{2} \begin{bmatrix} e^{j\Theta_1} & Z_1 e^{j\Theta_1} \\ e^{-j\Theta_1} & -Z_1 e^{-j\Theta_1} \end{bmatrix} \begin{bmatrix} V_1(z_0) \\ I_1(z_0) \end{bmatrix} \tag{126}$$

$$\begin{bmatrix} V_N(z_N) \\ I_N(z_N) \end{bmatrix} = \begin{bmatrix} 1 & 1 \\ Y_N & -Y_N \end{bmatrix} \begin{bmatrix} V_N^+ \\ V_N^- \end{bmatrix} \tag{127}$$

Using the relations (123) and (127) we obtain:

$$\frac{1}{2} \begin{bmatrix} 1 & \overleftarrow{Z}_N \end{bmatrix} \begin{bmatrix} 1 & 1 \\ Y_N & -Y_N \end{bmatrix} [\boldsymbol{T}] \begin{bmatrix} e^{j\Theta_1} & Z_1 e^{j\Theta_1} \\ e^{-j\Theta_1} & -Z_1 e^{-j\Theta_1} \end{bmatrix} \begin{bmatrix} \overrightarrow{Z}_1 \\ 1 \end{bmatrix} I_1(z_0) = 0 \tag{128}$$

This can be simplified into:

$$\underbrace{\begin{bmatrix} 1 + \dfrac{\overleftarrow{Z}_N}{Z_N} & 1 - \dfrac{\overleftarrow{Z}_N}{Z_N} \end{bmatrix}}_{\text{Termination}_N} [\boldsymbol{T}] \underbrace{\begin{bmatrix} \big[\overrightarrow{Z}_1 + Z_1\big] e^{j\Theta_1} \\ \big[\overrightarrow{Z}_1 - Z_1\big] e^{-j\Theta_1} \end{bmatrix}}_{\text{Termination}_1} = 0 \tag{129}$$

Hence, the final dispersion relation becomes:

$$\big[\boldsymbol{M}_N\big] \big[\boldsymbol{T}\big] \big[\boldsymbol{M}_1\big] = 0 \tag{130}$$

The dispersion relation in (130) is required to be analytic. Thus, the terminations 1 and N as in Table 1 and 2 must be strictly applied in order to avoid spurious zeros. Thus, the only problem left is to navigate through the Riemann sheets.

4.2 Modal Fields Profile

In order to evaluate the fields profile, we use the TL solutions after substituting the eigenvalue k_ρ. Here, we force the solution in section 1 as follows:

$$\begin{aligned} V_1(z) &= V_1^+ \big[e^{-jk_{z1}(z-z_1)} + \overrightarrow{\Gamma}_1 e^{jk_{z1}(z-z_1)}\big] \\ Z_1 I_1(z) &= V_1^+ \big[e^{-jk_{z1}(z-z_1)} - \overrightarrow{\Gamma}_1 e^{jk_{z1}(z-z_1)}\big] \end{aligned} \tag{131}$$

Table 1: Terminations for e TL.

	PEC	PMC	Semi-infinite
$\left[\boldsymbol{M}_1\right]$	$\begin{bmatrix} Z_1^e e^{j\Theta_1} \\ -Z_1^e e^{-j\Theta_1} \end{bmatrix}$	$\begin{bmatrix} Z_1^e e^{j\Theta_1} \\ Z_1^e e^{-j\Theta_1} \end{bmatrix}$	$\begin{bmatrix} Z_1^e \\ 0 \end{bmatrix}$
$\left[\boldsymbol{M}_N\right]$	$\begin{bmatrix} 1 & 1 \end{bmatrix}$	$\begin{bmatrix} 1 & -1 \end{bmatrix}$	$\begin{bmatrix} 1 & 0 \end{bmatrix}$

Table 2: Terminations for h TL.

	PEC	PMC	Semi-infinite
$\left[\boldsymbol{M}_1\right]$	$\begin{bmatrix} e^{j\Theta_1} \\ -e^{-j\Theta_1} \end{bmatrix}$	$\begin{bmatrix} e^{j\Theta_1} \\ e^{-j\Theta_1} \end{bmatrix}$	$\begin{bmatrix} 1 \\ 0 \end{bmatrix}$
$\left[\boldsymbol{M}_N\right]$	$\begin{bmatrix} \frac{1}{Z_N^h} & \frac{1}{Z_N^h} \end{bmatrix}$	$\begin{bmatrix} \frac{1}{Z_N^h} & -\frac{1}{Z_N^h} \end{bmatrix}$	$\begin{bmatrix} \frac{1}{Z_N^h} & 0 \end{bmatrix}$

Then, we continue using the down-looking solution discussed earlier. Using the boundary condition at z_1 we obtain the relation:

$$V_2^- = \frac{1 + \overrightarrow{\Gamma}_1}{1 + \overleftarrow{\Gamma}_2 e^{-j2\Theta_2}} V_1^+ \tag{132}$$

5 Numerical Results

Here, we demonstrate several numerical results for various configurations.

5.1 Paulus Configuration

This configuration is summarized as in Table 3 where $\overrightarrow{\Gamma}_1 = \overleftarrow{\Gamma}_N = 0$. The first results is the reflectivity on this configuration from top and bottom as shown in Figure 12. The second results are the TLGFs solutions including the direct ray. These sample results are illustrated in Figure 13 and 14. Samples of the DGFs are given in Figure 15.

Table 3: Paulus configuration details with $N = 4$ and $\lambda_0 = 633$ [nm]. All media are non-magnetic.

n	z_n [nm]	ϵ_n
0	1000	–
1	500	1
2	0	2
3	−500	10
4	−1000	1

5.2 Chew Configuration

The second configuration is summarized in Table 4 with semi-infinite layers 1 and 7, $\overrightarrow{\Gamma}_1 = \overleftarrow{\Gamma}_N = 0$. Here, we only demonstrate the electric fields due to arbitrary electric and magnetic point sources as illustrated in Figure 16.

5.3 Gold Kretschmann Configuration

The third configuration can support SPP modes given in Table 5. There are two TM modes, $k_\rho/k_0 = 1.04831197090811 - j0.00084271984542$ and $k_\rho/k_0 = 1.71377356475061 - j0.02971548827039$ that can be found using

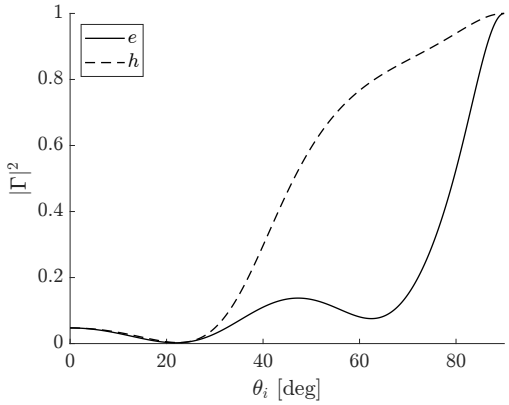

Figure 12: Reflectivity from top layer.

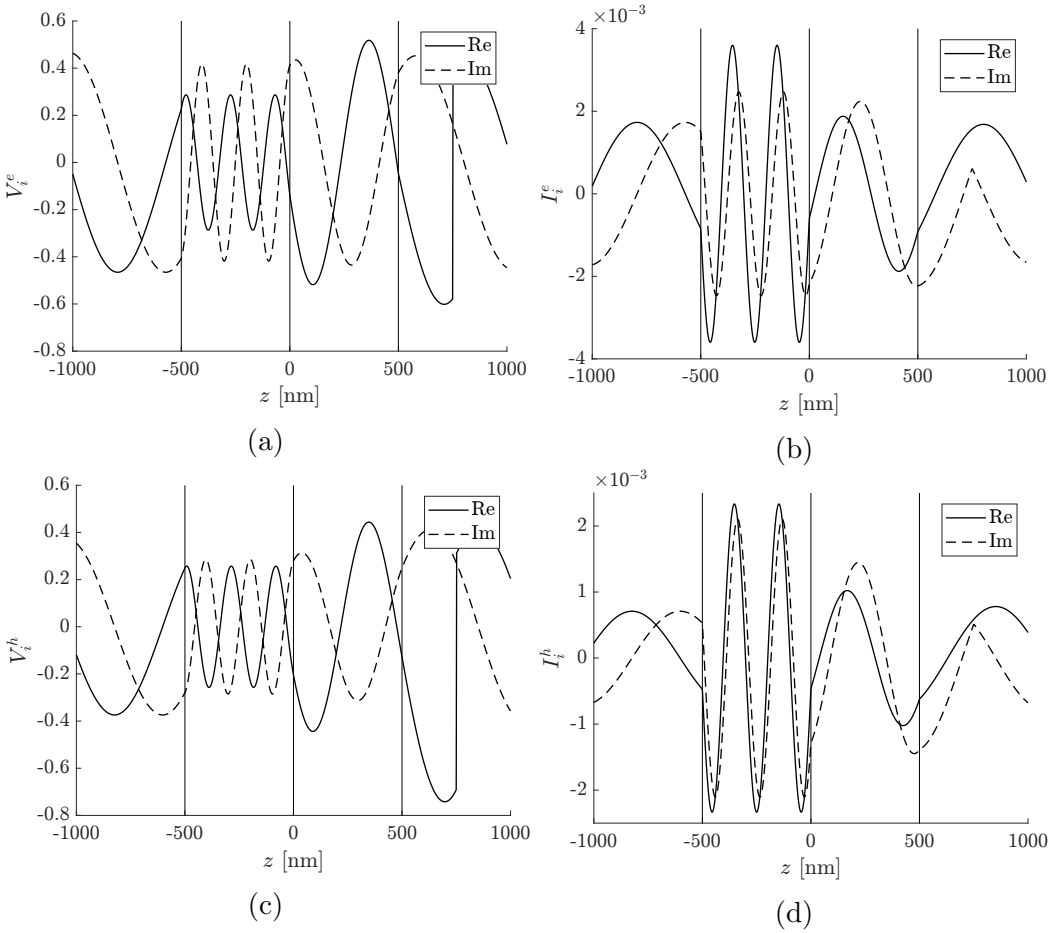

Figure 13: TLGF solutions for $z' = 750$ [nm] and $k_\rho = 0.7k_0$ due to a series voltage source v.

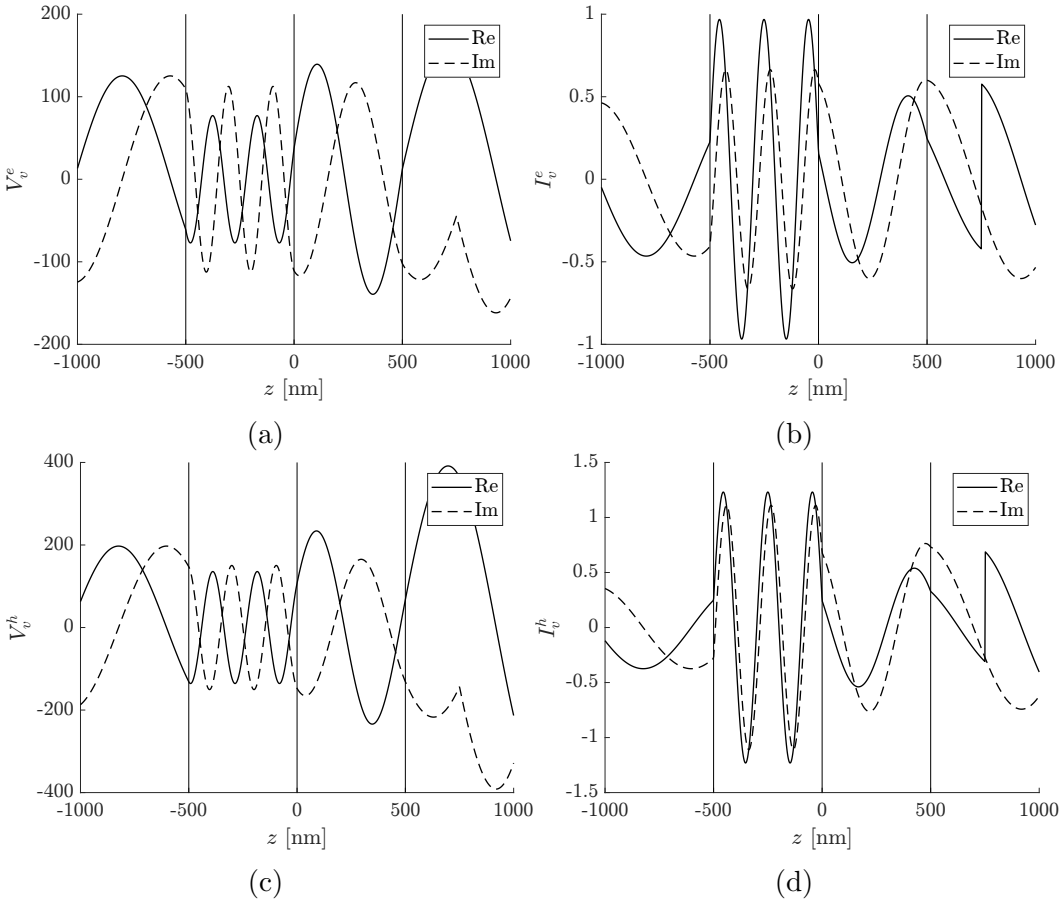

Figure 14: TLGF solutions for $z' = 750$ [nm] and $k_\rho = 0.7k_0$ due to a shunt current source i.

Table 4: Chew configuration details with $N = 7$ and $\lambda_0 = 1$ [m].

n	z_n [m]	μ_n	ϵ_n
0	10	–	–
1	0	1	1
2	-0.2	1	2.6
3	-0.5	3.2	6.5
4	-1	6	4.2
5	-1.3	3.2	6.5
6	-1.5	1	2.6
7	-10	1	1

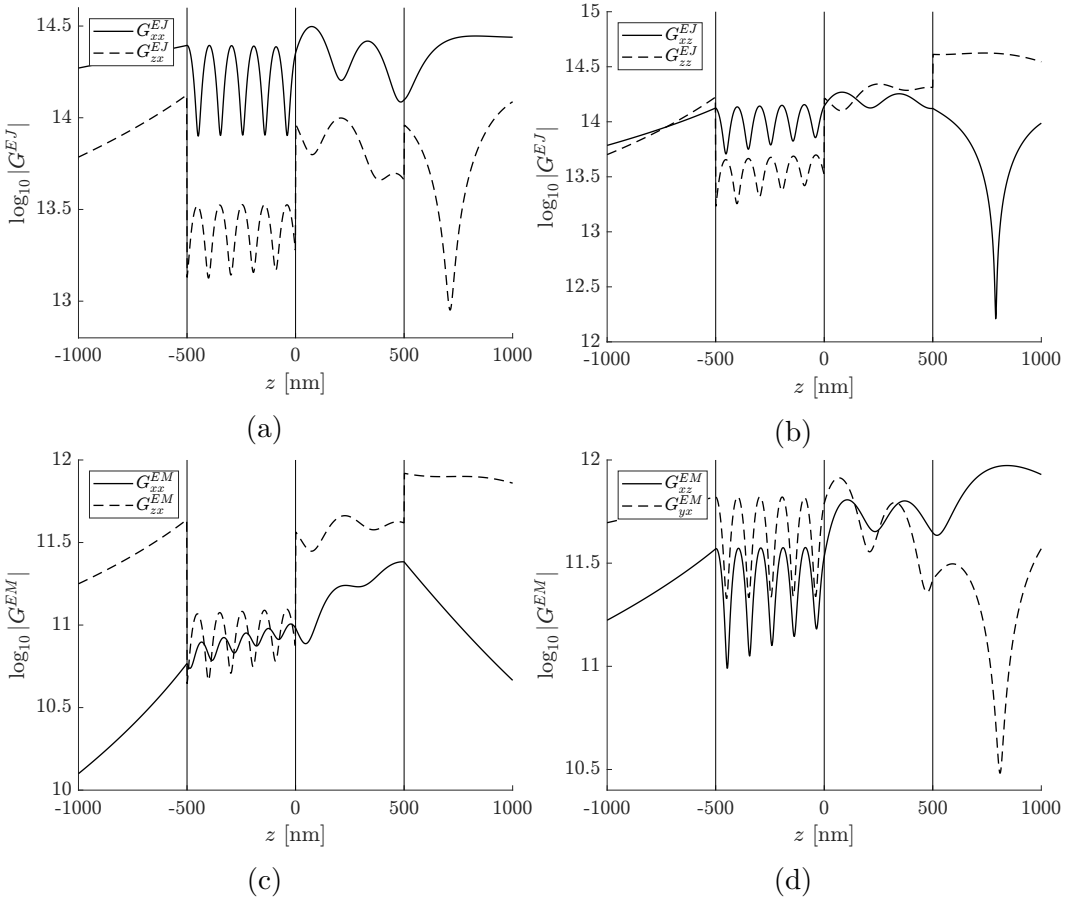

Figure 15: Dyadic Greens Functions for sources placed at $z' = 750$ [nm]. The observation is at $\rho = \lambda_0$, $\varphi = 45°$, and -1000 [nm] $\leq z \leq 1000$ [nm].

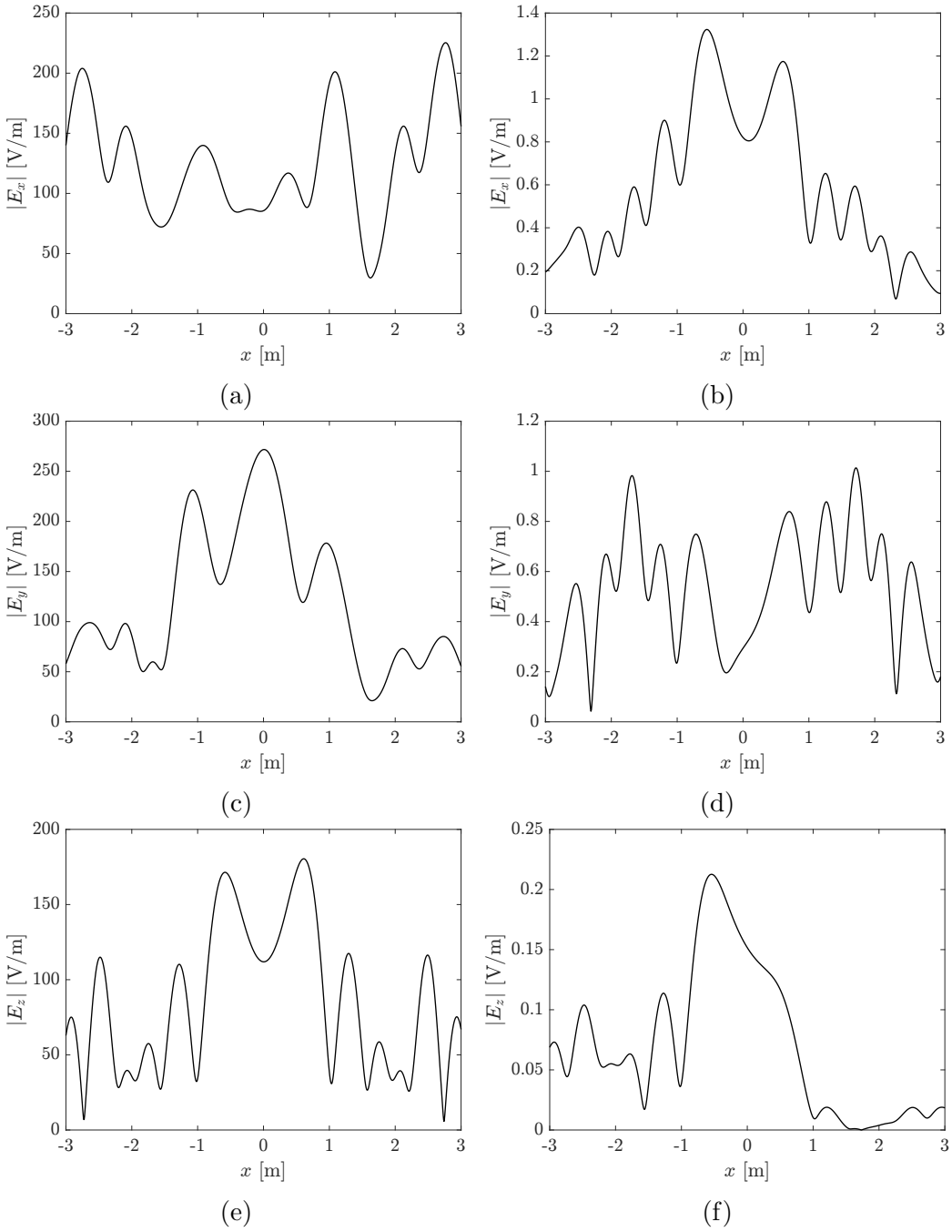

Figure 16: Electric fields due to dipoles at $z' = -1.4$ [m] with orientation $(\theta_0, \varphi_0) = (20°, 30°)$. The observation is -3 [m] $\leq x \leq 3$ [m], $y = 1$ [m], and $z = -0.3$ [m]. Left results are for $\boldsymbol{J}$ and right for $\boldsymbol{M}$ dipoles.

CIM described above. The SPP mode is associated with the first low losses pole. The reflectivities are shown in Figure 17 with a strong dip at $\theta_i \approx 43.7°$ for the TM plane waves. The excitation of the SPP mode by incident plane wave is shown in Figure 18. A 2D plot of the total electric field due to a point source is illustrated in Figure 19.

Table 5: Gold Kretschmann configuration details with $N = 3$ and $\lambda_0 = 633$ [nm]. All media are non-megnetic.

n	z_n [nm]	ϵ_n
0	2000	–
1	0	2.3013
2	−50	$-11.753 - j1.2596$
3	−2000	1

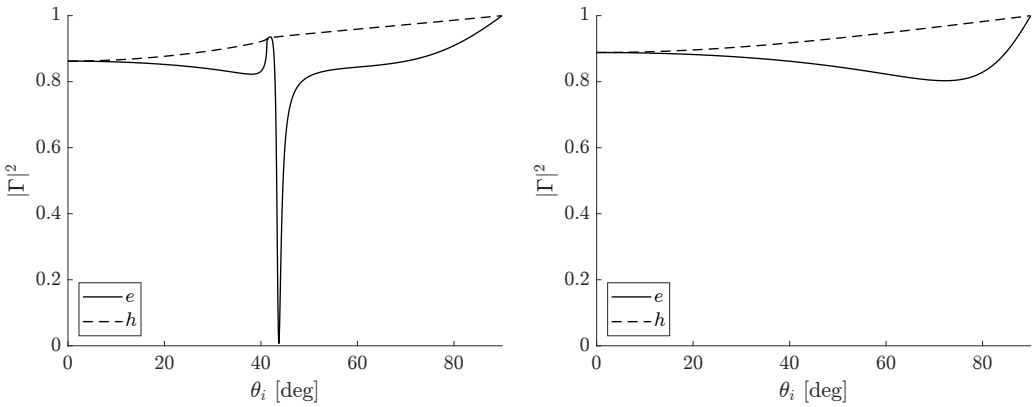

(a) (b)

Figure 17: Reflectivity illustrating TM SPP mode evaluated from top layer (b) bottom layer.

5.4 Visser Configuration

This configuration is summarized in Table 6. Here, we studied the proper sheet modal fields eigenvalues as listed in Table 7. Examples of the modal fields profiles are illustrated in Figure 20.

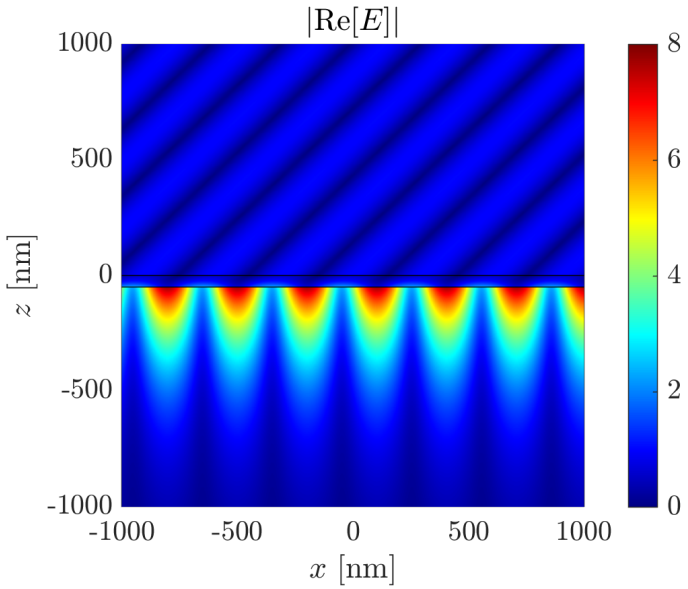

Figure 18: Electric field due to TM incident plane wave at $\theta^i = 43.7°$.

Table 6: Visser configuration details with $N = 5$ and $\lambda_0 = 1.3$ [μm]. All media are non-megnetic.

n	z_n [μm]	$\sqrt{\epsilon_n}$
0	0	–
1	0	1
2	-0.6	$3.4 - j0.002$
3	-1	$3.6 + j0.01$
4	-1.6	$3.4 - j0.002$
5	-1.6	1

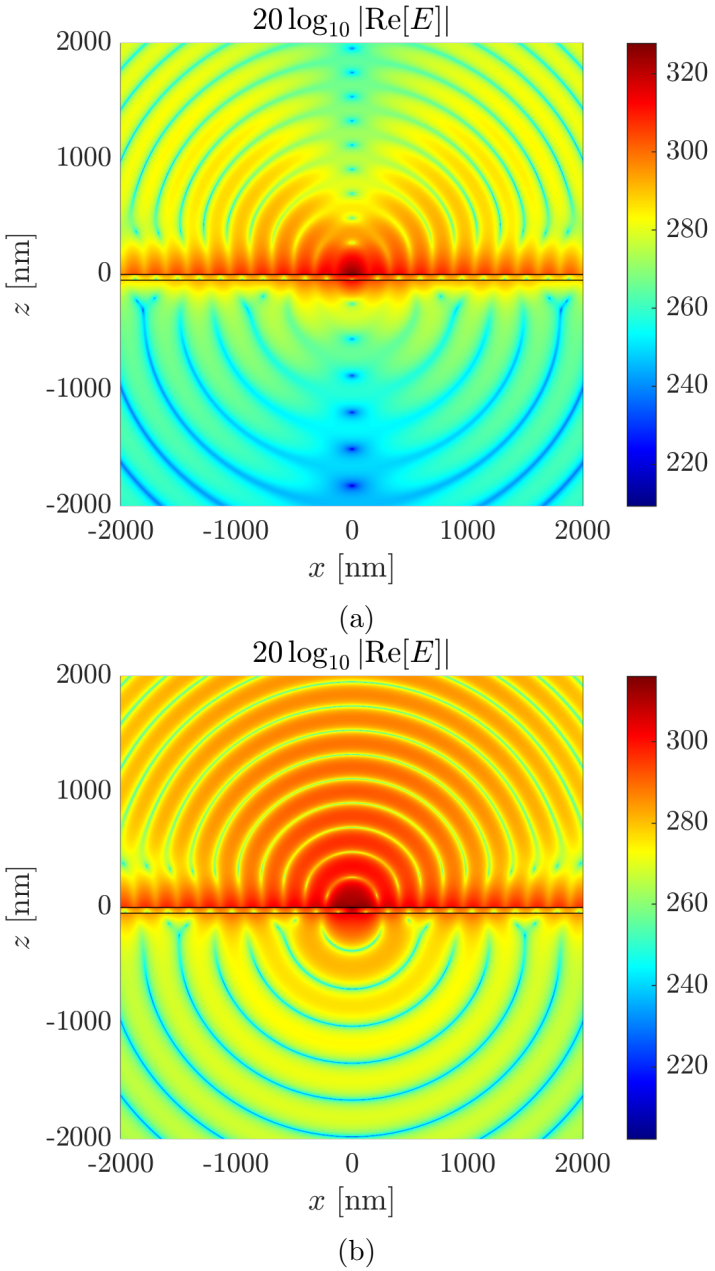

Figure 19: Electric field at $z' = 20$ [nm] due to (a) VED (b) HED.

Table 7: k_ρ eigenvalues for TE and TM modes on Sheet I.

Mode	k_ρ/k_0
TE_1	$3.50344333295000 + j0.00710300097870$
TE_2	$3.33728685820780 - j0.00022949110400$
TE_3	$3.25168520698340 - j0.00053051477990$
TE_4	$3.10425142141457 + j0.00133798633975$
TE_5	$2.87863677988123 - j0.00017372989036$
TE_6	$2.62813932045903 + j0.00154864433115$
TE_7	$2.24395136260119 + j0.00070837795801$
TE_8	$1.76819096041243 + j0.00135321718386$
TE_9	$1.07426202652578 + j0.00245789147357$
TM_1	$3.49668379589130 + j0.00654398171100$
TM_2	$3.33069711910720 + j0.00003518642230$
TM_3	$3.22433799874650 - j0.00017448261260$
TM_4	$3.05040586521867 + j0.00117031512099$
TM_5	$2.79439777568252 + j0.00070878520448$
TM_6	$2.46292446281425 + j0.00117932006477$
TM_7	$2.00514007332263 + j0.00160292202929$
TM_8	$1.35099878658162 + j0.00231404951497$
TM_9	$1.00143843982593 + j0.00004669412354$

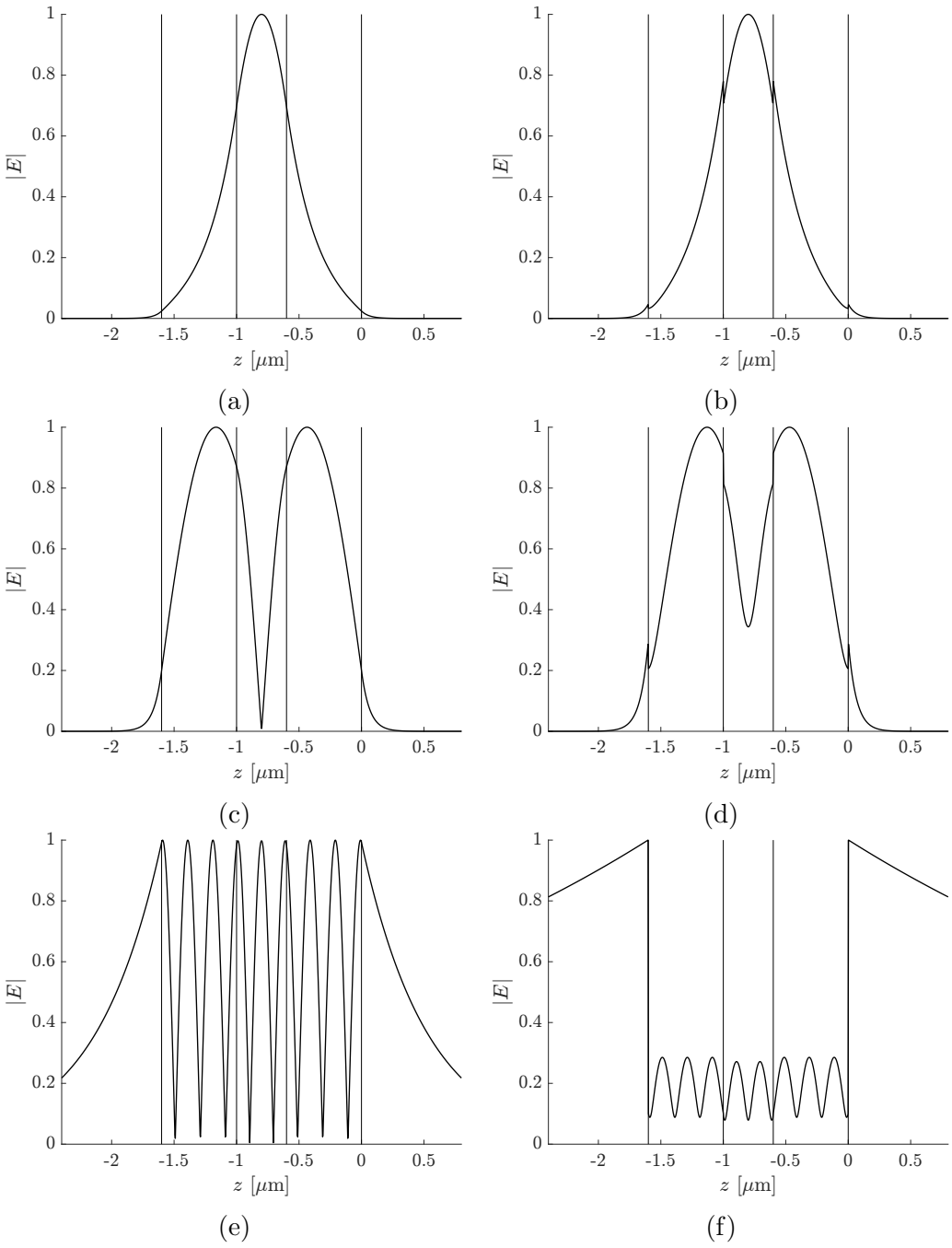

Figure 20: Normalized electric field profiles corresponding to the modes in Table 7. (a) TE_1 (b) TM_1 (c) TE_2 (d) TM_2 (e) TE_9 (f) TM_9.

5.5 Otto-Graphene Configuration

The following configuration is summarized in Table 8. The reflectivity is shown in Figure 21. The SPP excitation by incident plane wave is illustrated in Figure 22. The SPP modal field profile is shown in Figure 23 and the far-fields at various distances in Figure 24.

Table 8: Otto-Graphene configuration details with $N = 3$ and $f = 1$ [THz]. All media are non-megnetic and $\sigma_n^s = 0$ except $\sigma_2^s = 3.69059545723 \times 10^{-4} - j1.5237384931248 \times 10^{-2}$ [S].

n	z_n [μm]	$\sqrt{\epsilon_n}$
0	1000	–
1	0	2.003
2	−20	1
3	−1000	1.762

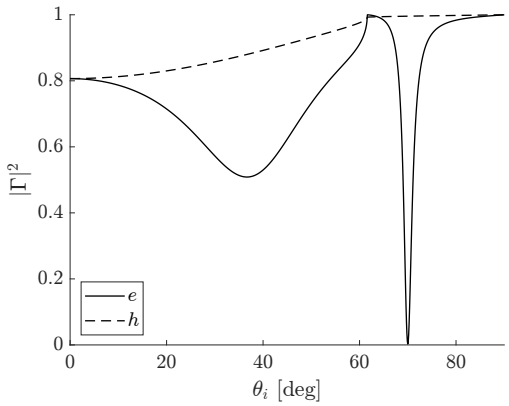

Figure 21: Reflectivity from top layer.

5.6 Miscellaneous Configurations

Two more results are given for different configurations. The first one in the incident plane wave electric field in Figure 25 for the plasmonic waveguide configuration from Table 9. The second configuration is given in Table 10 is associated with the far-fields in Figure 26.

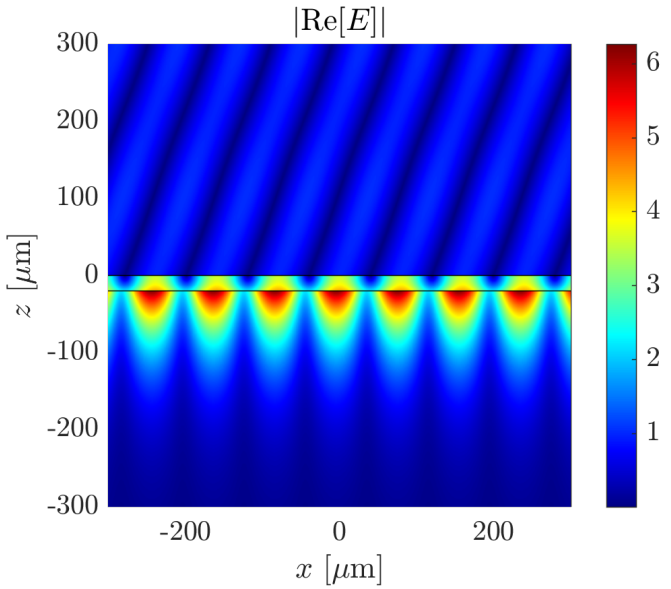

Figure 22: Electric field due to TM incident plane wave at $\theta^i = 70°$.

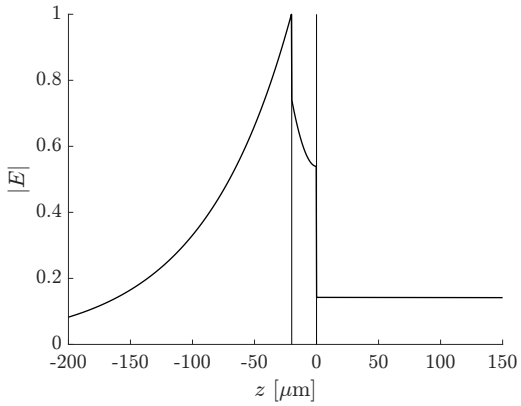

Figure 23: Electric field profiles associated with the SPP mode $k_\rho/k_0 = 1.88224222918665 - j0.00063471402154$.

Table 9: Plasmonic waveguide configuration details with $N = 4$ and $\lambda_0 = 633$ [nm]. All media are non-megnetic.

n	z_n [nm]	ϵ_n
0	2000	–
1	50	2.3013
2	0	$-18.5698 - j0.397$
3	-30	2.07
4	-2000	1.79

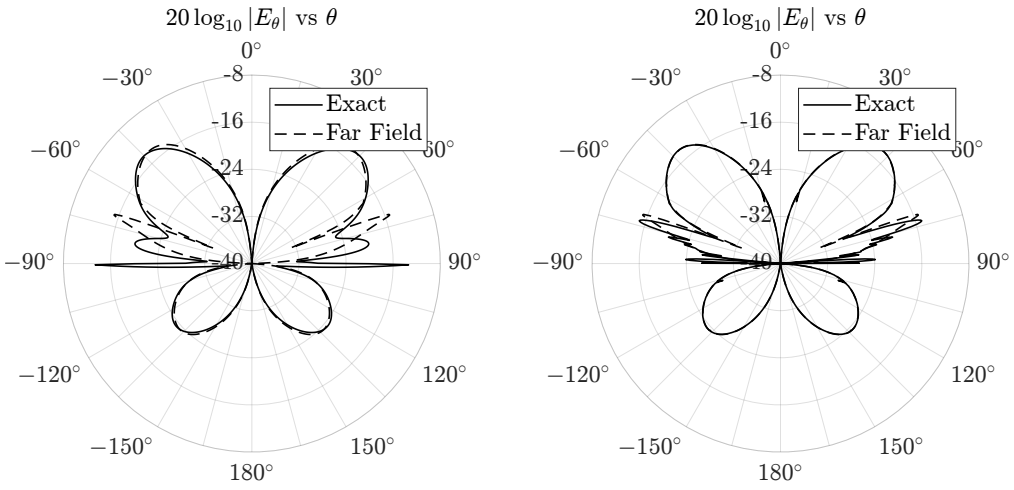

Figure 24: Electric field due to a VED placed at $z' = 5$ [μm] compared to far-field approximation. The observation is a θ-cut with radius R surrounding the dipole at $\varphi = 0°$. Results were normalized by $\sqrt{2\eta_0}$ in order to represent power and multiplied by R to remove distance effect. (a) $R = 10\lambda_0$ (b) $R = 100\lambda_0$.

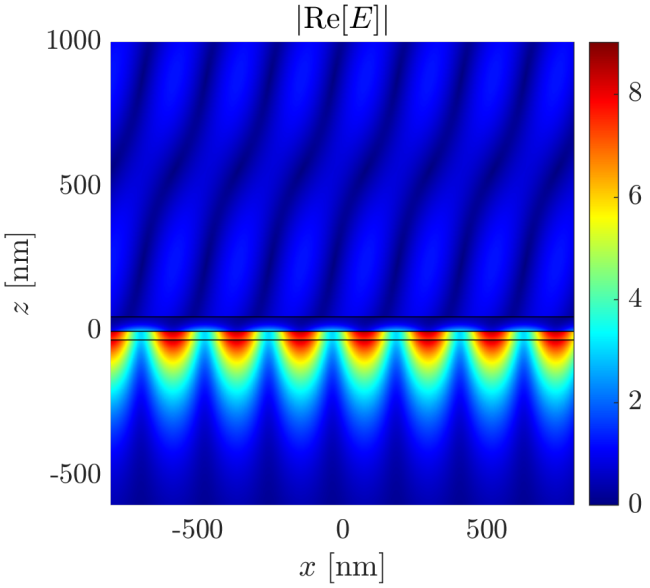

Figure 25: Electric field due to TM incident plane wave at $\theta^i = 71.1°$.

Table 10: Glass Bragg configuration details with $N = 19$ and $\lambda_0 = 633$ [nm]. All media are non-megnetic.

n	z_n [nm]	ϵ_n
0	2500	–
1	1523	2.3013
2	1445	4.5967
3	1329	2.1229
4	1241	4.5967
5	1115	2.1229
6	1037	4.5967
7	911	2.1229
8	833	4.5967
9	707	2.1229
10	629	4.5967
11	503	2.1229
12	425	4.5967
13	299	2.1229
14	221	4.5967
15	69	2.1229
16	42	2.1229
17	0	$-18.3511 - j0.4331$
18	-27	2.1229
19	-500	1

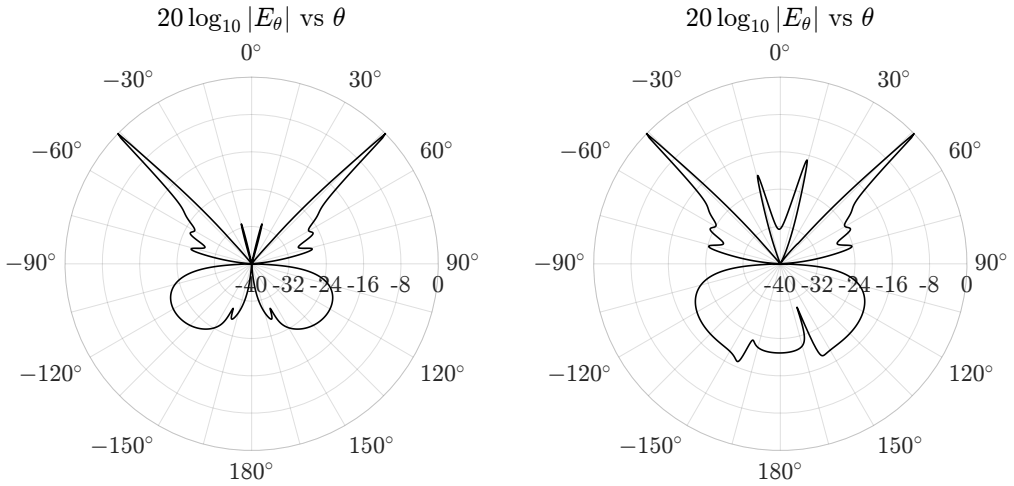

Figure 26: Far-field E_θ due to dipoles at $z' = -15$ [nm] with orientation $(\theta_0, \varphi_0) = (135°, 0°)$. The observation is a θ-cut at fixed φ (a) $\varphi = 0°$ (b) $\varphi = 90°$.